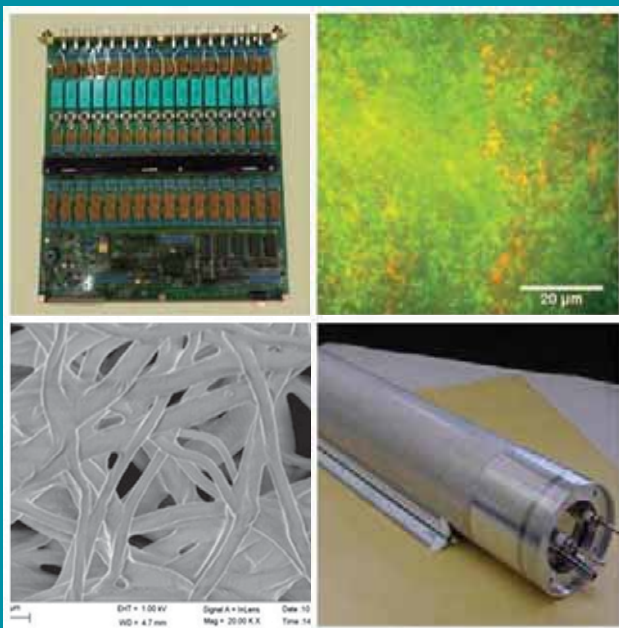# BARC
NEWSLETTER

भाभा परमाणु अनुसंधान केंद्र
BHABHA ATOMIC RESEARCH CENTRE

IN THIS ISSUE

- Atomic, Molecular and Cluster Physics with an Indigenously Developed Supersonic Molecular Beam

- Synthetic and Structural Studies of Uranyl Complexes

- Development of Hybrid Micro Circuit Based Multi-Channel Programmable HV Supply for BARC-Pelletron Experimental Facility

- Xenon Transport in Uranium-10wt% Zirconium Alloy

- Diffusion Bonding of Nuclear Materials

- Microwave Processing in Thorium Fuel Cycle

- Emergent Biofilm Control Strategies Based on Controlled Release of Antimicrobials: Potential Industrial and Biomedical Applications

In the Forthcoming Issue

CONTENTS

From the Editor's Desk

The March-April Issue of the BARC Newsletter is with you. This issue carries 7 articles and 4 Brief Communications. It also carries reports of several scientific events conducted by various Divisions of BARC.

The Research articles from Chemical Sciences domain include, transport kinetics of fission product Xenon in Uranium-Zirconium alloy, which is important for the analysis of high burnup performance, structural studies of uranyl complexes and the application of microwave heating in Thorium-based fuel cycle. In the field of Physical Sciences, an indigenous laser vaporization supersonic molecular beam experimental setup has been included. A report of Atomic, Molecular and Cluster Physics studies conducted using this setup, has been described in one of the articles. In the area of Electronics, details of development of a Multi channel programmable HV bias supply system for charge particle detector array, for use in the BARC-TIFR Pelletron-LINAC facility is included. In the area of Material Sciences, one of the Research articles provides an overview of diffusion bonding, which has emerged as an advanced technique for joining similar and dissimilar materials.

His Excellency Mr. Yukiya Amano, Director General, IAEA visited BARC on March 11, 2013 and he inaugurated an exhibition on the theme "Atoms in the Service of the Nation". Young scientists and engineers interacted with Mr. Amano and presented posters on BARC's contributions in the field of health, environment, food, water, industry and agriculture. A detailed description of this event is included in this issue.

We are happy to inform all the Scientists and Engineers of BARC that a dedicated hyperlink has been developed, for direct uploading of articles for the BARC Newsletter and I am sure that this facility will strengthen our communication and help timely publication of the BARC Newsletter.

Dr. K. Bhanumurthy
On behalf of the Editorial Committee

Prostate Cancer Treatment Using 'BARC I-125 Ocuprosta Seeds'

(Radiochemistry and Isotope Group)

Transperineal Interstitial Permanent Prostate Brachytherapy (TIPPB) is an outpatient radioactive seed implantation procedure, to deliver a tumoricidal dose to the patient for the treatment of prostate cancer. 'BARC I-125 Occu-prosta seeds' were developed by the Radiopharmaceuticals Division for the treatment of Ocular and Prostate cancer, and is in use for the treatment of ocular cancers since 2003. The first use of these seeds for treatment of prostate cancer was done at the P.D. Hinduja National Hospital & Medical Research Centre, Mumbai in September 2011. The sources are fabricated by using ^{125}I produced in the Dhruva reactor and is based on the adsorption of ^{125}I on palladium coated silver rods of 0.5mm (ϕ) × 3 mm (l) followed by laser encapsulation in titanium tubes and quality control tests to ensure safety. The sources were qualified by preclinical bioevaluation studies in rabbits at ACTREC. 'Classification Performance Validation' of the seeds as per AERB specifications was done prior to use in patients. Implantation of the sources was done in a patient who had stage II prostate cancer of adenocarcinoma histology. Patient received 50 Gy to the prostate and proximal seminal vesicles over 5 weeks by external beam radiation therapy (IMRT technique). Patient underwent Transrectal Ultrasound (TRUS) image based pre-plan, on which dose distribution was virtually generated by using Treatment Planning Simulator (TPS). Forty-three seeds having an average strength of ~0.36 mCi each were implanted into the prostate under real time TRUS image and fluoroscopic guidance to deliver a dose of 110 Gy to the prostate gland. The patient is doing well post therapy.
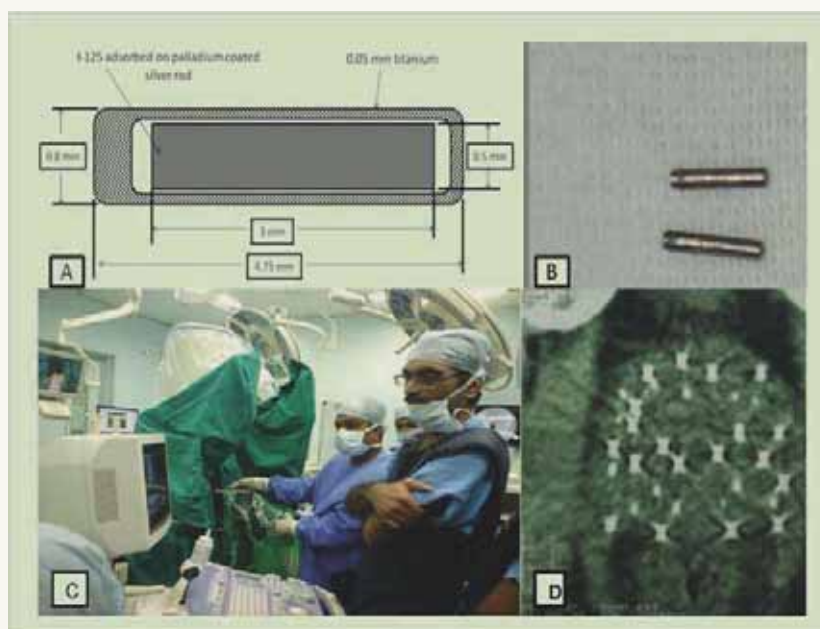
Fig.: Transperineal Interstitial Permanent Prostate Brachytherapy (TIPPB) treatment. A. Schematic diagram of 'BARC I-125 Ocuprosta seeds'; B. Iodine-125 seeds; C. Seeds implantation in progress; D. CT scan image of prostate with seeds.

Silver Nanoparticle Based Colorimetric Method for Sensitive Detection of Hg^{2+} in Aqueous System

(Chemistry Group)

A highly sensitive and selective method has been developed for the colorimetric detection of aqueous Hg^{2+} by using label - free silver nanoparticles (Ag NPs). The Ag NPs used were synthesized by gum kondagogu (GK) which acted as both reducing as well as stabilizing agent. The synthesized GK-Ag NPs were directly used for the selective colorimetric reaction with Hg^{2+} without any further modification. The bright yellow color of silver nanoparticles fades rapidly with the addition of Hg^{2+}. The fading response could be directly correlated with increasing concentration of Hg^{2+}. The intensity of absorbance of the Ag nanoparticles reduced with increased concentration of Hg^{2+} ions. More importantly, this response was found to be highly selective for Hg^{2+} as the absorption spectra was found to be unaffected by the presence of other ions like; Na$^+$, K$^+$, Mg^{2+}, Ca^{2+}, Cu^{2+}, Ni^{2+}, Co^{2+}, As^{3+}, Fe^{2+}, Cd^{2+} etc. The synthesized GK- Ag NPs were found to be stable in various pH, salt concentrations and in different matrices. The method was successfully applied for the quantitative determination of Hg^{2+} in various ground water samples. The detection limit of Hg^{2+} by this method was as low as 10 ppb. Further, it has also been demonstrated that the proposed method can be used for the determination of total mercury in the samples, with the assistance of UV irradiation.
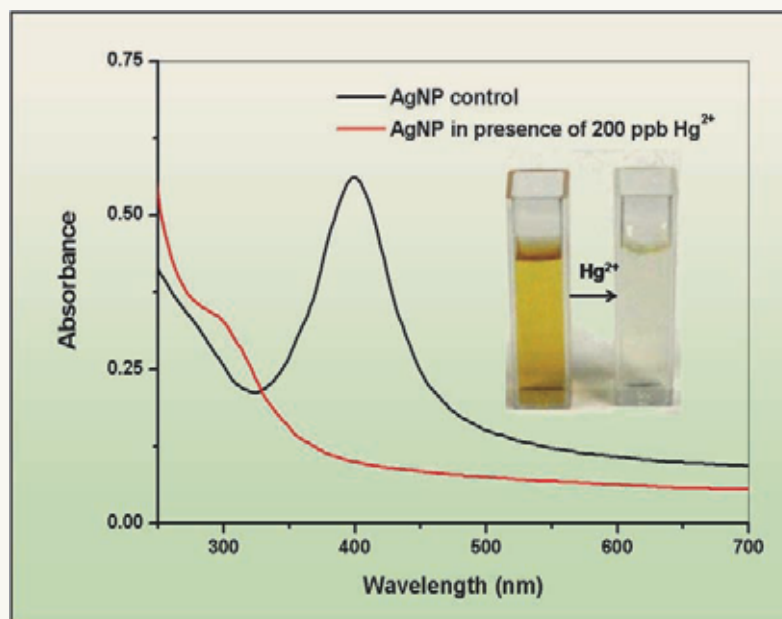
Fig.: UV-visible spectra of as synthesized GK-Ag NPs and Ag NPs in the presence of 200 ppb of Hg^{2+} ions. Inset: photograph showing colour change of Ag NPs from yellow to colourless after Hg^{2+} addition.

Two-Dimensional Infrared (2DIR) Spectrometer

(Chemistry Group)

Normally the conventional (1D) infrared spectra of polyatomic molecules are complex and spectrally congested for achieving high spectral and spatial resolutions. The coupling between different bonds are sensitively dependent on the three dimensional molecular structure and cannot be obtained from such conventional spectra. Recent development of the two dimensional (2D) infrared spectroscopy overcomes this limitation and the vibrational coupling between different modes is identified through the appearance of the off-diagonal peak in the 2D IR spectrum (Fig. 1). The strength of such off-diagonal peak is a measure of the extent of coupling and hence the spatial separation between two coupled bonds. Such coupling can take place through space, through covalent and non-covalent interactions. Detail polarization dependent study can further reveal the relative direction of the coupled bonds.

The present 2D IR spectrometer is developed and commissioned in the Radiation & Photochemistry Division around a 1kHz amplified 100 femtosecond Ti-Sapphire laser system (Fig. 2&3). The infrared laser pulses generated in Optical Parametric Amplifiers (OPA) and Difference Frequency Generators (DFG) are used for the excitation and probing of the sample. In the present setup, a wide range of wavelengths (2-8 micron) are available for the interrogation of the sample and hence the coupling between various vibrational bonds can be studied. Due to use of femtosecond laser pulses, time resolution of the 2DIR instrument is sufficient to monitor ultrafast structural motion in the chemical and biological systems involving chemical exchange reactions, solution dynamics, hydrogen network evolution, intramolecular vibrational energy relaxations, protein structures and dynamics, supramolecular interactions, etc.
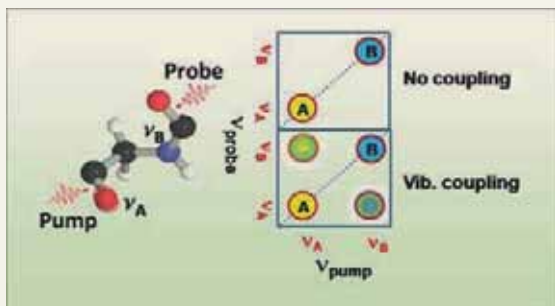
Fig.1: 2D IR spectrum
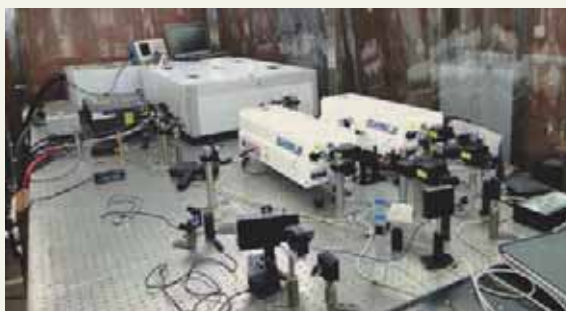
Fig. 2:The 2D IR spectrometer
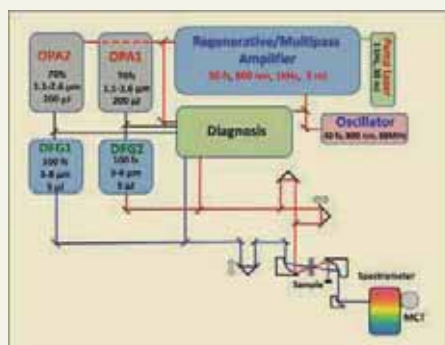
Fig. 3: Schematic of the 2D IR spectrometer

Wavelet Analysis as New Tool for Understanding Earthquake Ground Motion

(Reactor Design and Development Group)

Safety of the nuclear facilities has to be ensured under low probable earthquakes. The ground motion generated during an earthquake is random and non-stationary with respect to both amplitude and frequency. Fourier analyses are the most commonly used tools for signal processing of ground motion. It helps in extracting frequency and amplitude information of the ground motion and it does not give any information about the time at which various frequency components of the motion occurs. It is not robust in analyzing the sharp spikes or discontinuities in a signal.

Wavelet analysis has emerged as a powerful tool to study the ground motion characteristics, generation of random time histories of ground motion and evaluation of non-stationary stochastic site response. The wavelet analysis procedure utilizes basis functions which are scaled and translated versions of mother wavelets such as Morlet, Daubechies and Harr Wavelets. Long time intervals give more precise low frequency information whereas shorter time intervals give high frequency information. In the present work, Morlet wavelet is used to understand the recorded accelerograms. Recorded accelerogram of Kobe earthquake is shown in Fig.1. Fig. 2 shows the Fourier spectrum of the accelerogram and the wavelet representation of the same signal is given in Fig. 3. Wavelet representation shows time, frequency and amplitude information of the signal simultaneously and also provides the time of occurrence of dominating frequencies. The projected 2D plots of wavelet spectrum in time and frequency domain are shown in Fig. 4. It can be seen that the frequency and amplitude plot is same as obtained in Fourier analysis. The response of structures under extreme design earthquake motions will be different if the occurrence of low and high frequencies in the ground motion is altered. Hence, time of occurrence of dominating frequencies is to be taken into account for generation of design basis ground motion. This information is vital for the seismic design of safety related structures systems and components. These aspects need to be taken care of even in the case of generating test time histories compatible to the design spectrum used for qualifying components and systems.

Fig. 1: Recorded accelerogram

Fig. 3: Wavelet representation

Fig. 2: Fourier spectrum

Fig. 4: Projected 2D plots of wavelet spectrum
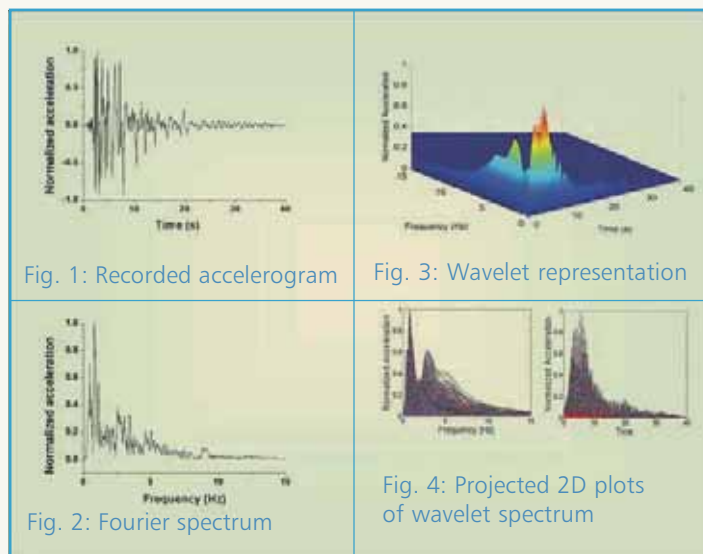
Synthetic and Structural Studies of Uranyl Complexes

S. Kannan
Fuel Chemistry Division

Abstract

The complex chemistry of uranyl nitrate with mono and bi-functional neutral extractants shows, that it forms 1:2 and 1:1 complexes respectively. The structures of the isolated complexes show, that the water molecules from the primary coordination sphere of $[UO_2(NO_3)_2.2H_2O]$ are replaced by the extractants completely and adopt a hexagonal bi-pyramidal geometry. However, the structural chemistry of uranyl nitrate with the tri-functional extractants show, that one of the nitrates acts as a monodentate ligand to maintain the hexagonal bi-pyramidal geometry. The complex chemistry of uranyl bis(β-diketonates) with the neutral monodentate extractants shows that the water molecule from the primary sphere of $[UO_2(β\text{-diketonate})_2.H_2O]$ is replaced by the ligands, to form a pentagonal bi-pyramidal geometry around uranyl group. However, the structural chemistry of bi-functional neutral extractants with uranyl bis(β-diketonats) shows either mono or bi-nuclear uranyl complexes depending upon the stoichiometry of the uranyl ion used.

Introduction

The coordination chemistry of uranium is growing rapidly in the recent years due to the presence of new synthetic methods [1-2] and also interesting properties such as selective ion-exchange, mixed valence, ionic conductivity, enhanced fluorescence, magnetic ordering and nonlinear optical properties exhibited by its complexes. The basic understanding of the coordination chemistry of the uranyl group is very important for the selective complexation and separation of this ion from the acid medium during reprocessing of irradiated AHWR nuclear fuel, biological and environmental samples [3]. Various new extractants were developed for the above mentioned purposes in the last two decades and their extraction and coordination chemistry were studied. This article will give a brief report on the synthetic and structural studies of the uranyl complexes with the extractants, which are used in the separation studies.

Coordination numbers and Geometries of actinide complexes

Since, there is no ligand field effect on 5f orbitals, the coordination number and hence the geometry around the actinide ions will be decided mainly by the charge and size of the metal ions as well as the size of the ligands used and not by the crystal field effects as seen in the transition metal ions. Actinide ions display relatively large ionic radii and therefore support higher coordination numbers of 12 to 14 which are not seen in the transition metal ions. The coordination chemistry of uranyl ion is relatively simpler compared to those of spherical ions, due to the presence of a linear uranyl group (O=U=O). The coordination number around the uranyl group varies from 3 to 6 and leads to trigonal bi-pyramidal to hexagonal bi-pyramidal geometries.

Structural studies on complexes related to separation science and technology

Separation of actinides particularly uranium and plutonium from the irradiated nuclear fuel and americium from high level waste solution, by using variety of neutral extractants such as, phosphine oxides, phosphates and amides, has been well reported. Various types of neutral extractants having different donor groups have been studied and they were classified according to the number of donor centers present in the molecule, such as mono-functional, bi-functional, tri-functional etc . The coordination, extraction and structural properties of these extractants are completely different from each

other giving interesting geometries around the metal ions.

Coordination and Structural Study of neutral Extractants

Neutral mono-functional extractants

Tri-n-butyl phosphate is used as an extractant for the separation of uranium and plutonium from the irradiated nuclear fuel in PUREX process. Studies on the extraction of uranium, plutonium and neptunium from nitric acid medium using neutral mono-functional extractants such as, phosphine oxides, phosphates and amides have been reported. In all these processes, the extraction mechanism could be written as follows:

$[UO_2(NO_3)_2. 2H_2O] + 2 L \rightarrow [UO_2(NO_3)_2. 2L] + 2H_2O$
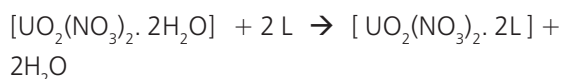
L = Phosphine oxides, Phosphates, N-oxide or Amides

These reactions are basically inorganic substitution reactions, in which the water molecules from the primary coordination sphere are replaced by the neutral donor ligands. For many of the extraction processes, the species responsible for the same are isolated in the solid state and characterized by using IR, ^{1}H NMR spectroscopy, elemental analysis and for some of the compounds by using the single crystal x-ray diffraction method.

The IR spectra of the isolated complexes show that the disappearance of v_{OH} peak around 3000- 3500 cm^{-1} is due the presence of the coordinated water molecules in the starting complex $[UO_2(NO_3)_2. 2H_2O]$. The spectra further show that the ligands are bonded through the functional groups such as P=O and C=O respectively for the phosphine oxides, phosphates and amides to the metal centers (there will be a decrease in frequencies of P=O and C=O groups compared to that of free ligand after complexation). The elemental analysis revealed that the ligands form 2:1 complex with uranyl nitrate, in all the cases.

The crystal structure for the starting compound $[UO_2(NO_3)_2.2H_2O]$ (Fig.1a) is reported and shows that the water molecules are directly bonded to the metal center. On reaction with two equivalent of neutral ligands these water molecules are completely replaced from the primary coordination sphere as shown in Fig.1b.

The structures for the complexes $[UO_2(NO_3)_2(OPBu_3)_2]$ [4], $[UO_2(NO_3)_2(N$-alkyl pyrrolidone$)_2]$ [5] and $[UO_2(NO_3)_2(^iC_3H_7CON\{^iC_4H_7\}_2)_2]$ [6] were determined by using single crystal x-ray diffraction methods and confirm the solvent extraction, spectral and elemental analysis data. The structures show that the metal ions are surrounded by two nitrate
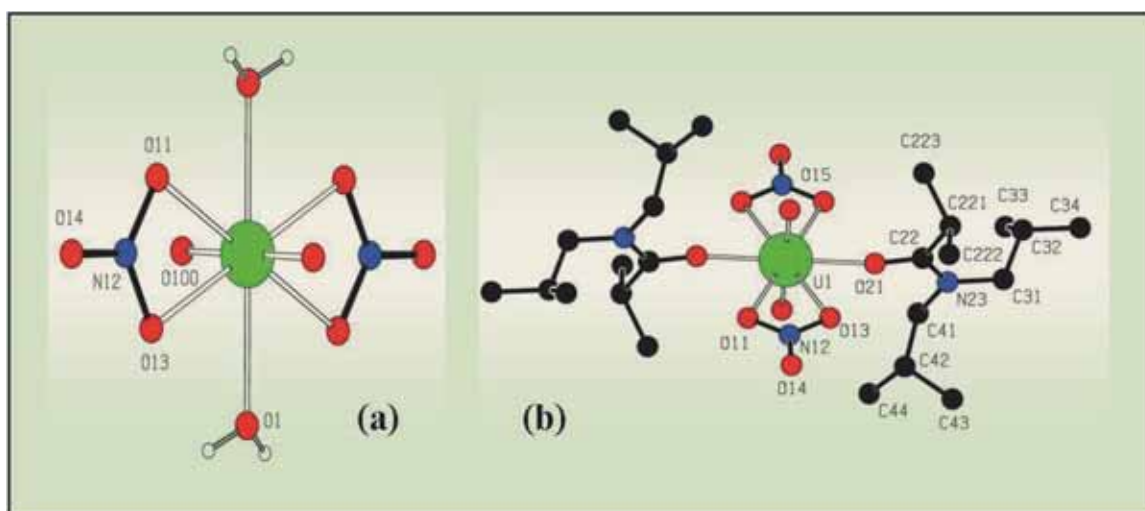
Fig. 1: Structure of (a) $[UO_2(NO_3)_2.2H_2O]$ and (b) $[UO_2(NO_3)_2. (Amide)_2]$

groups, two mono-functional neutral extractants and two oxygen atoms to give a coordination number eight and a hexagonal bi- pyramidal geometry. Four oxygen atoms from two nitrate groups and two oxygen atoms from two neutral ligands form a planar hexagon and two oxygen atoms of O=U=O group occupy the axial positions.

Neutral bi-functional extractants

The extraction properties of many bi-functional extractants, such as carbamoyl methyl phosphonates (CMP), carbamoyl methyl phosphine oxides (CMPO), malonamides and bis(diaklyl phosphino methane) dioxides, carbamoyl methyl sulfoxides (CMSO) and carbamoyl methyl pyrazole (CMPz) with the actinide ions from the nitric acid medium have been studied extensively. The species responsible for these extractions were determined using solvent extraction methods. The mechanism for this extraction process can be written as.

$[UO_2(NO_3)_2. 2H_2O] + 2L \rightarrow [UO_2(NO_3)_2. 2L] + 2H_2O$
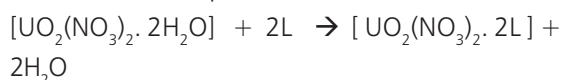
The complexes responsible for the extraction process were prepared by reacting the respective nitrates with the bi-functional ligands in a required ratio and the final products were characterized by using the IR, ^{1}H, ^{31}P (only for phosphorus containing ligands) NMR spectroscopy and elemental analysis.

The ^{31}P NMR of the complexes show the ^{31}P resonance in the complexes is deshielded by 20 -30 ppm with respect to the free ligands. This confirms the coordination of phosphine oxide group with the metal centre. The ^{1}H NMR shows that all protons are deshielded with respect to free ligand in the complexes and in particular CH_2 protons (CH_2 bridging the PO and CO in CMP and CMPO or CO and CO in malonamides) are more deshielded compared to other protons. These observations support the coordination of ligands to the metal ion in solution.

The IR spectra further support that the ligands are bonded through both the carbamoyl and phosphine oxide groups to the metal centre in the solid state. However, in most of the complexes, the elemental analysis results show, that the stoichiometry of the complexes isolated in the solid state are different from those of the solvent extraction. In many cases, the metal to ligand ratio in the solid state structure (1:1) is different from that of the solvent extraction (1:2) results. However, the ESMS studies on the solid state compounds in solution revealed that the compounds undergo disproportionation to give a mixture of both 1:1 and 1:2 complexes. This confirms that the solid state structure is different from that of the proposed solution structure.
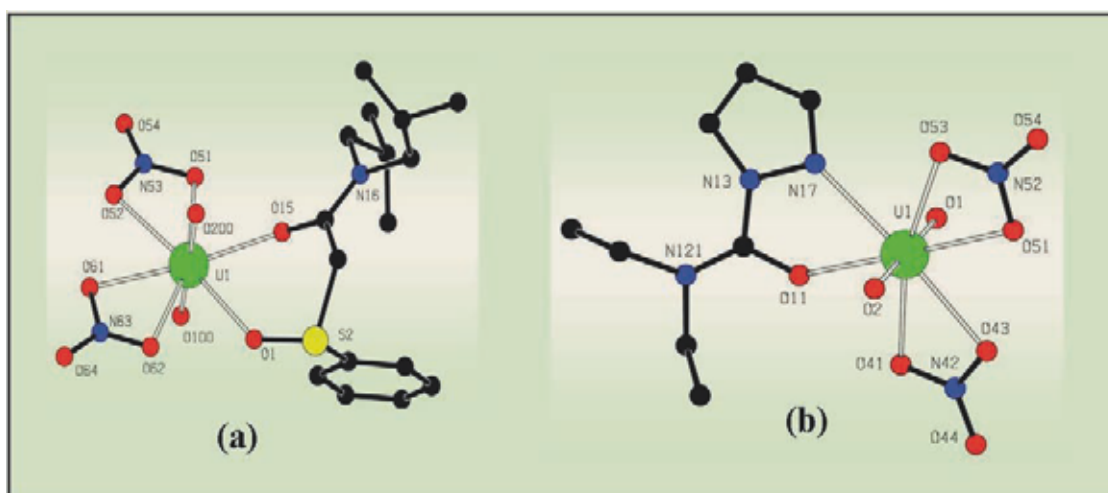
Fig. 2: Structure of (a) [UO_2(NO_3)_2. CMSO] and (b) [UO_2(NO_3)_2.CPz]

The structures for number of complexes were determined by using the single crystal x-ray diffraction method to confirm the spectral and elemental analysis data. The structure of complexes $[UO_2(NO_3)_2.CMPO]$,$[UO_2(NO_3)_2CMP]$ [7] $[UO_2(NO_3)_2.$ malonamide] [8], $[UO_2(NO_3)_2.CMSO]$ [9], $[UO_2(NO_3)_2.CMPz]$, [10] $[UO_2(NO_3)_2.CPz]$ [11] and $[UO_2(NO_3)_2.($ bis-phophine oxide)] [12] shows that the uranyl group is bonded to two nitrates and one neutral bi-functional ligands, to give a hexagonal bi-pyramidal geometry [Fig. 2]. The four oxygen atoms from two nitrate groups and two oxygen atoms from the neutral ligands form a planar hexagon and two uranyl oxygens occupy the axial positions.

Tri-functional neutral extractants

The structure of uranyl nitrate di-glycolamide complex is also isolated in the solid state and characterized by x-ray diffraction method. The structure of $[UO_2(NO_3)_2L]$ [13] shows that the uranyl group is bonded to two nitrates and one di-glycolamide ligand. The di-glycolamide ligand acts as a tridentate chelating ligand and is bonded through both the carbamoyl and ethereal oxygen atoms to the uranyl group [Fig.3]. Three oxygen atoms from the di-glycolamide ligand and three oxygen atoms from two nitrate groups form a planar hexagon. The two uranyl oxygens occupy the axial positions. However, the reaction of thio-diglycolamide or bis
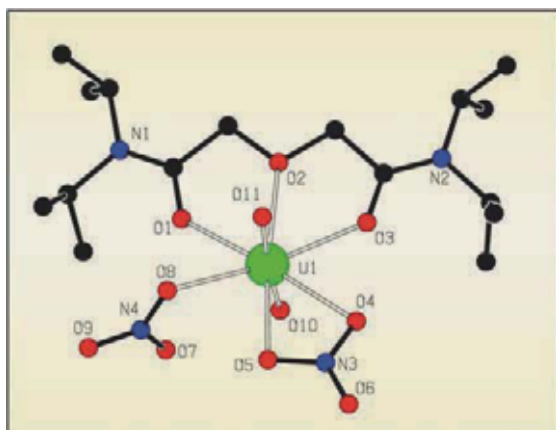
Fig. 3: Structure of $[UO_2(NO_3)_2.$ DGA]

(carbamoylmethyl) sulfone [14] with the uranyl nitrate shows a bidentate chelating mode of bonding for these ligands and bond through carbamoyl oxygen atoms to the uranyl nitrate. The reaction of bis(carbamoyl methyl) sulfoxide [15] with uranyl nitrate shows bidentate chelating mode of bonding with the uranyl nitrate and bonds through the sulfoxo and carbamoyl groups.

Synergistic Extraction of Uranyl Ion using a Mixture of β-diketones and Neutral Extractants

The synergistic extraction of uranyl ion from the acid media by using the mixture of β-diketones and neutral extractants is a well established method. The increase in extraction is due to the formation of a more organic soluble complex of uranyl ion with both the β-diketones and neutral extractants. The mechanism for this process could be written as follow:

UO_2^{2+} + n2LH + A $\rightarrow$ [UO_2L_2A] + $2H^+$

(L = diketonate anion and A = neutral extractant)

Structural studies on uranyl ion-β-diketonate-neutral extractant complexes

A large numbers of complexes of actinide ions with the combination of β-diketonates and neutral extractants have been prepared in the solid state and characterized by using the spectroscopic and elemental analysis methods. The structures for many of the uranyl complexes show that the uranyl group is bonded to two of the β-diketonate anions and one neutral extractant [12] . The coordination number and geometry around the uranyl group is seven and pentagonal bi-pyramidal respectively [Fig.4]. It is interesting to note that the observed bond distance between the oxygen atom of the neutral ligands to the uranyl group follows the order of: Phosphine oxides < Phosphates < sulfoxides < amides < N-oxides < ketones. This observation is consistent with the observed basicity of the neutral extractants.

A large number of complexes containing the combination of β-diketones and neutral bi-functional
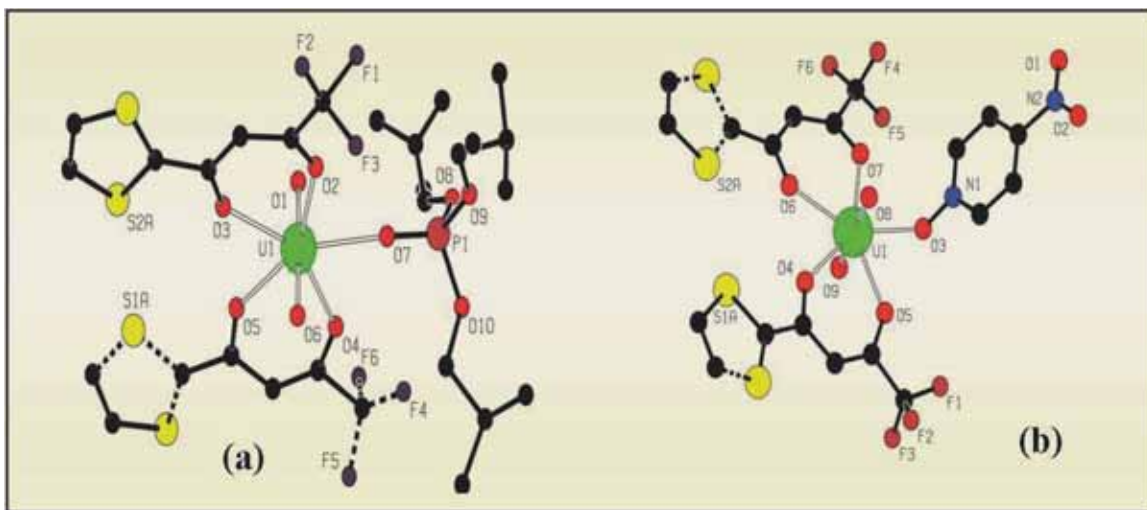
Fig. 4: Structures of (a) [UO$_2$(TTA)$_2$.(TIBP)] and (b) [UO$_2$(TTA)$_2$.PyNO]

extractants have also been isolated and characterized by IR and NMR spectroscopy. In most of the cases the bi-functional ligands act as monodentate ligands and bond through the most basic donor group. For example, in cases of CMP or CMPO, they bonded only through the more basic PO groups rather than the weak carbamoyl group revealed from the spectroscopic data. The ^{31}P NMR spectra of the complexes of CMPO or CMP with uranyl bis (β-diketonates) show that the ^{31}P resonances are deshielded by 20 – 30 ppm with respect to the free ligand. This confirms the coordination of PO group to the uranyl group. The IR spectra of the complexes

show that the carbamoyl group is free (uncoordinated). The monodentate mode of bonding for the bi-functional neutral extractant was established in one of the compounds [UO$_2$(DBM)$_2$.{(C$_6$H$_5$)$_2$P(O)CH$_2$}$_2$] [12]. The structure of the complex shows that the uranyl group is surrounded by two dibenzoyl methanate anions and one bi-functional neutral donor diphenylphosphino methane dioxide [Fig 5(a)]. The neutral ligand acts as a monodentate ligand and bonds through only one of the phosphine oxide groups. However, the 2:1 reaction of [UO$_2$(DBM)$_2$.H$_2$O] with the same
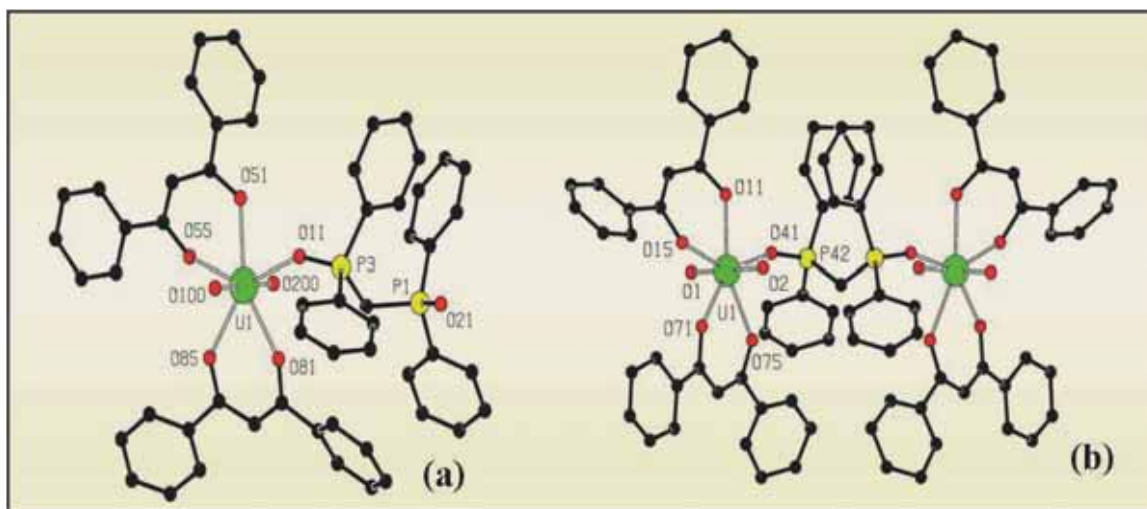
Fig. 5: Structure of (a) [UO$_2$(DBM)$_2$.DPPMO$_2$] and (b) [{UO$_2$(DBM)$_2$}$_2$DPPMO$_2$]

ligand yielded a dinuclear compound in which the ligand acts as a bridging bidentate ligand [Fig 5(b)].

Conclusions

The structural studies on the uranyl complexes revealed that the coordination number and geometry around the metal ion are mostly decided by the size of the ligands used. These studies support (in most of the cases, particularly when mono functional extractants are in use) the structures, which have been proposed on the basis of solvent extraction results. The observed bond lengths between the neutral ligands and the uranyl ion agree well with the basicity of the neutral ligands used.

Acknowledgements

References

1. M. B. Jones and A. J. Gaunt, *Chem.Rev*, 113 (2013) 1137-1198.

2. M. Ephritikhine, *Dalton Trans*. (2006) 2501-2516.

3. G. R. Choppin, K. L. Nash, *Radiochim. Acta*, 70/71 (1995) 225-236.

4. J. H. Burnes, *Inorg. Chem*. 20 (1981) 3868-3871.

5. N. Koshino, M. Harada, M. Nogami, Y. Morita, T. Kikuchi, Y. Ikeda, *Inorg. Chim. Acta* 358 (2005) 1857-1864.

6. S.Kannan, S. B. Deb, J.S. Gamare, M.G.B. Drew, *Polyhedron,* 27 (2008) 2557-2562

7. L. J. Caudle, E. N. Duesler, R. T. Paine, *Inorg. Chim. Acta*, 110 (1985) 91- 100.

8. G. J. Lumetta, B. K. McNarma, B. M. Rapko, R. L. Shell, R. D. Rogers, G. Broker, J. E. Hutchison, *Inorg. Chim. Acta,* 309 (2000) 103- 108.

9. S.Kannan, K. V. Chetty, V. Venugopal, M. G. B. Drew, *Dalton Trans.* (2004) 3604 -3610.

10. S. Kannan, J.S. Gamare, K.V. Chetty, M.G.B. Drew, *Polyhedron*, 26 (2007) 3810 - 3816.

11. D. Das, S. Kannan, D. K. Maity, M. G. B. Drew, *Inorg.Chem.* 51 (2012) 4869 – 4876.

12. S. Kannan, N. Rajalakshmi, K.V. Chetty, V. Venugopal, *Polyhedron*, 23 (2004) 1527-1533.

13. S. Kannan, M. A. Moody, C. L. Barnes, P.B. Duval, *Inorg.Chem*. 47 (2008) 4691-4695.

14. S.B. Deb, J.S. Gamare, S. Kannan, M. G. Drew, *Polyhedron*, 28 (2009) 2673-2678.

Atomic, Molecular and Cluster Physics with an Indigenously Developed Supersonic Molecular Beam

S.G. Nakhate, Sheo Mukund and Soumen Bhattacharyya
Atomic & Molecular Physics Division

Abstract

An indigenous laser vaporization supersonic molecular beam experimental setup has been developed. The setup has been extensively used for studying the electronic structures of transition metal-containing diatomic molecules and for measuring radiative lifetime of atoms. It has been also used to study the metal clusters.

Introduction

The utility of molecular beam for spectroscopic and collision studies of atoms and molecules is well known [1]. Over the years, a number of different strategies have been employed to produce gaseous metal atoms and ions, namely thermally heated oven sources including the ones with added collision gases, discharge sputtering sources and electrospray ionization to name a few. The laser vaporization source, also known as the "Smalley source", developed in 1981 by Smalley and co-workers [2], has made it possible to produce a wide variety of refractory metal clusters and refractory metal-containing molecules. The capability of the pulsed laser to vaporize highly refractory elements in combination with supersonic jet where the plasma, generated by laser vaporization, is expanded directly into the supersonic helium flow through small tube, cools the metal and thereby promotes condensation to form clusters of various sizes. Supersonic expansion cools the internal degrees of freedom of molecules and thereby simplifies the spectrum.

Since the initial demonstration, the laser vaporization source has been employed for investigating a wide range of applications related to metal-containing molecules and clusters, and its versatility has proven to be quite remarkable. Over the last decade and half, considerable progress has been made in understanding the electronic structure of transition metal-containing species. Transition metal-containing diatomic species have been the subject of many theoretical and experimental studies in order to understand the bonding in simple systems and, particularly, the interaction of transition metals with hydrogen, carbon, nitrogen, and oxygen. Transition metal-containing diatomics provide models to help in our understanding of bonding and reactivity in transition metal systems.

Keeping in view the versatility of this technique to generate cold beam of atoms, molecules and clusters of elements of refractory material, we have developed the laser ablation supersonic molecular beam setup in our laboratory in the 11th plan project. The experimental facility has Laser-Induced Fluorescence (LIF) as well as linear Time-Of-Flight Mass Spectrometer (TOFMS) detection. The facility has been utilized to address a wide range of problems in atomic (lifetime measurement of zirconium and lanthanum atoms), molecular (LIF spectroscopy in jet-cooled LaH, ScN, ScO) and cluster (LaO) physics. The article is divided into two parts. The first part provides discussions on the experimental setup and the second part deals with its utilization with a focus on molecular spectroscopy.

Experimental

a. Supersonic atomic/molecular free-jet with LIF detection

Fig. 1 shows a schematic of the experimental setup and a photograph of the set up is shown in Fig. 2. The vacuum chamber is a six-port double cross built with CF250 conflat flanges. It has additional four CF35 ports to insert vacuum gauges and ceramic vacuum feedthroughs. A home-made gas pulse valve is mounted on one of the CF250 flanges. The opposite port to the pulse valve is used to view the alignment of ablation laser beam on metal target. The side ports are used to insert the ablation and the dye laser beams. Laser induced fluorescence is collected from the top port by collection optics and imaged on the monochromator slit. The 10 inch throat turbomolecular pump (Pfeiffer vacuum TPU 2301) backed by a rotary vane pump (Pfeiffer vacuum DUO 65) is attached to the bottom port of the chamber through a pneumatically operated gate valve. The background pressure $<1 \times 10^{-7}$ mbar is regularly obtained. A vaporization source similar to the one used by Hopkins et al. [3] is fitted on the home built piezoelectric disc based gas pulse valve. The species being studied, for example Zr, in metal rod form having diameter 6 mm, positioned in front of a nozzle of about 350 micron diameter, which is rotated and translated by a motor driven micrometer screw. Free Zr metal atoms and ions were generated in a laser produced plasma by focusing the third harmonic of a Nd:YAG laser (Quanta System SYL 203) beam having pulse duration 8 ns and energy ~15 mJ on the zirconium rod. The Nd:YAG laser beam is passed through a 2 mm open channel in the vaporization source from a side-port of the chamber. The generated hot Zr metal plasma is cooled and recombined by a supersonic helium gas pulse emanating from the nozzle into a channel of diameter 2 mm and length 7 mm and expanded freely into the vacuum chamber. A typical helium
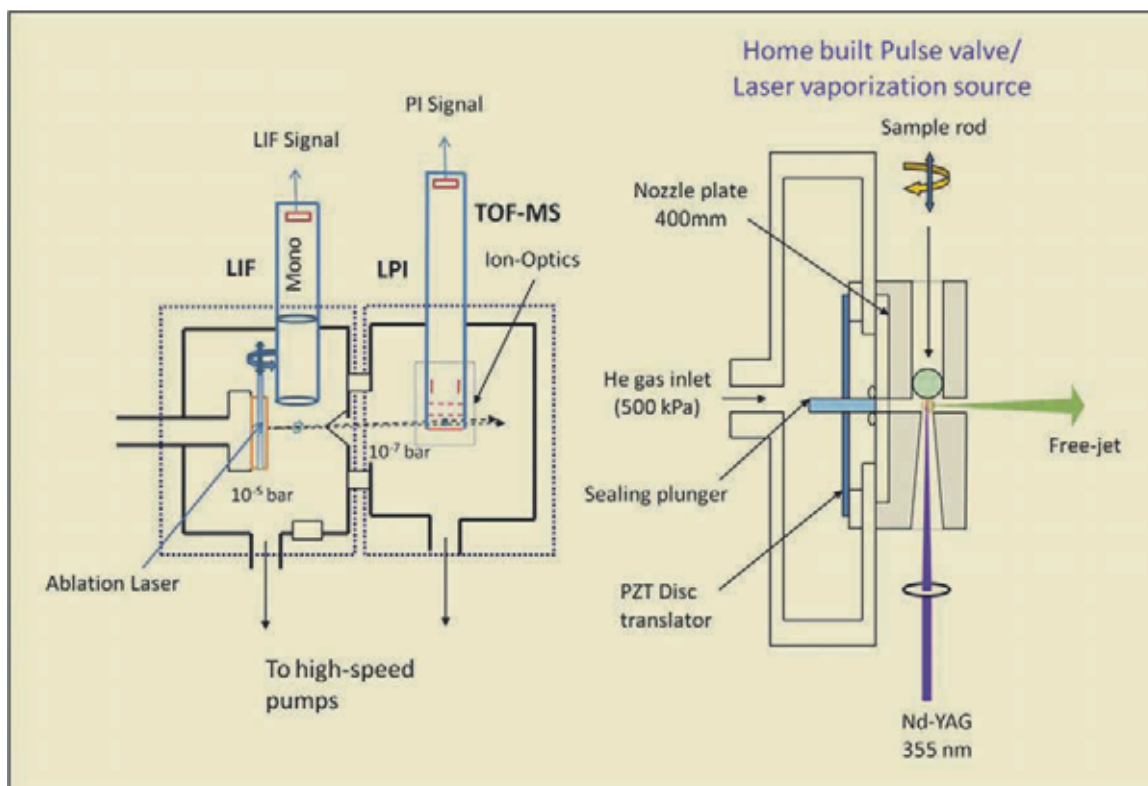
Fig.1: Schematic of the molecular beam setup. LIF: Laser induced fluorescence, LPI: Laser photoionization, TOF-MS: Time-of-flight mass spectrometer, Mono: Monochromator.

Fig. 2: Photograph of the supersonic molecular beam setup.

backing pressure of about 210 kPa is used. The pressure in the expansion chamber is $\sim 1 \times 10^{-5}$ mbar with the pulse valve operated at 10 Hz repetition rate. The translationally cooled metal atoms/molecules are excited by a tunable pulsed dye laser (Coherent ScanMatePro) pumped by a XeCl excimer laser (Coherent CompexPro 201) 50 mm downstream the nozzle. Typical pulse duration (FWHM) of the dye laser is 11 ns. Several dyes are used to cover tunability in few hundred nanometer range for an atomic lifetime measurements or for searching new electronic energy levels of molecules. The LIF is collected at right angles to the plane formed by the expansion axis and the excitation axis by means of a biconvex 5 cm $f/1$ quartz lens. The fluorescence collection optics images the intersection of the laser and atomic beams with magnification of 4 on the entrance slit of a monochromator (Spex 270M). The slit is aligned parallel to the atomic beam direction. The fluorescence is detected by a Peltier cooled photomultiplier tube (Hamamatsu R943-02). A black

anodized cone of aperture 3 mm diameter is attached in front of the collection lens to minimize the scattered light from excitation laser falling on the photomultiplier tube. The LIF signal is optimized by appropriately adjusting the time delays between the gas pulse, vaporization laser pulse and the dye laser pulse using a digital delay generator (Stanford Research System DG535). The excitation spectra of Zr atoms are recorded by detecting the resonance fluorescence while scanning the monochromator along the dye laser wavelength. The monochromator is used as a broadband filter by keeping the entrance and exit slits 2 mm wide. A boxcar averager (Stanford Research System SR250) is used to integrate 10 pulses and a data acquisition and controller system (Jobin Yvon Spex DataScan2) of the monochromator is used to acquire the data on a personal computer. Dispersed Fluorescence (DF) spectra are also recorded by keeping the excitation laser wavelength fixed and scanning the monochromator. While recording the DF spectra, the monochromator

entrance and exit slits are reduced to 0.2 to 0.5 mm to increase the resolution of the DF spectra. In an atomic lifetime measurement experiment, lifetimes of the excited states are recorded by acquiring the fluorescence decay curve on a 200 MHz digital storage oscilloscope (Tektronics TDS 2024) having sampling rate of 2 Giga-samples/s and rise time <2 ns. The decay curve is averaged for 128 shots in order to obtain a good signal-to-noise ratio.

b. Molecular beam with TOFMS detection

The free-jet is skimmed into a molecular beam to a second vacuum chamber separated from the source chamber by a gate valve and pumped by turbomolecular pump (Pfeiffer vacuum TPU 1201) backed by a rotary vane pump (Pfeiffer vacuum DUO 35). An indigenously built linear TOFMS with Wiley-McLaren ion-extraction optics having field-free drift length of 50 cm is mounted in perpendicular configuration on this chamber. Two side ports of this chamber are used for delivering the excitation/ionization laser beam. Fig. 3 shows the resolved zirconium isotopes as recorded in our TOFMS via resonant two-photon ionization. A typical mass resolution of this mass spectrometer is ~ 400.
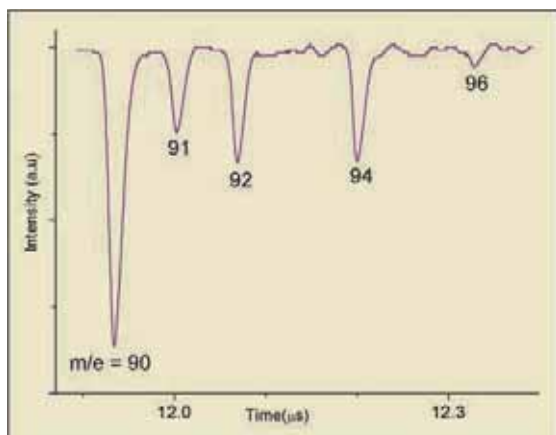
Fig. 3: Mass spectrum of zirconium atom recorded in our home built linear TOFMS observed by resonant two photon ionization.

Results and Discussions

a. Electronic structure of ScN molecule

Diatomic transition metal nitrides are simple model systems for studying nitrogen fixation in industrial,

inorganic, and biological systems. The only experimental studies of ScN reported in literature was one on the gas phase [4] and the other on the matrix isolation spectroscopy [5]. This motivated us to investigate the electronic structure of this molecule. The ground state was confirmed to have $^1\Sigma^+$ symmetry by analyzing LIF excitation spectra. We observed three new electronic states $B1$, $D1$ having $^1\Pi$ and $C1$ with $^3\Pi$ symmetry [6]. A typical rotational spectra showing PQR branch lines of (0,0) $C1$-$X^1\Sigma^+$ transition of ScN molecule is shown in Fig. 4. The fundamental vibration of the ground state was measured. The equilibrium internuclear distances and fundamental vibrations for the new electronic states were also determined. The new excited states could not be accounted by the existing *ab initio* results. The electronic structures of ScN and its isovalent YN are found to be similar.
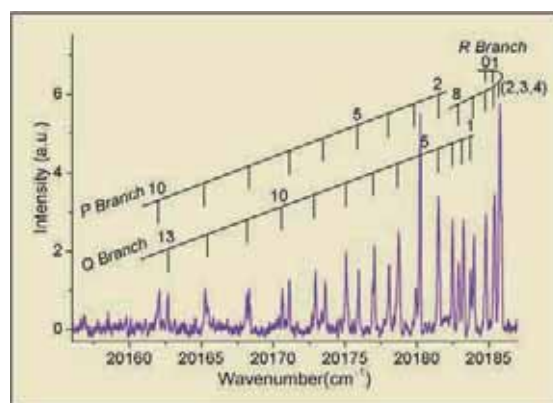
Fig. 4: Rotational structure of the (0,0) $C1$-$X^1\Sigma^+$ excitation band of jet-cooled ScN molecule.

Dispersed fluorescence studies resulted in the observation of the first excited state $a^3\Sigma^+$ of this molecule. The relative term energies of the vibrational levels of the $X^1\Sigma^+$ ground, $a^3\Sigma^+$, and $A^1\Sigma^+$ states were also determined [7]. RKR potential energy curves of the ground as well as low-energy excited states were constructed.

b. Singlet-triplet energy linkage in LaH and observations of new electronic states

The measurement of electron Electric Dipole Moment (eEDM) is a topic of current research [8] and LaH is a potential candidate for this. The molecule should

have a low-lying $^3\Delta$ metastable state for eEDM measurement. The ground state symmetry of LaH molecule was unambiguously assigned by our work [9]. Determination of the term energy of the $^3\Delta$ state established the missing singlet-triplet manifold energy linkage [10]. All the low energy states predicted by theoretical studies are now observed experimentally.

c. Improved molecular constants of $B^2\Sigma^+–X^2\Sigma^+$ system of ScO

The spectra of ScO molecule are of considerable astrophysical interest. Especially, the $B^2\Sigma^+–X^2\Sigma^+$ system of this band, which falls in the blue-green region of the electromagnetic spectra, were identified in the stellar spectra. A precise knowledge on equilibrium rotation, vibration constants and Frank Condon factors are thus essential for understanding many aspects of the molecule like rotational, vibrational temperature etc., which are related to the state of the emitting source. We have determined a set of improved equilibrium molecular constants for the electronic levels from the extensive set of molecular constants for individual vibrational levels [11]. RKR potential curves for both the states were constructed. The Frank-Condon factors for $B^2\Sigma^+–X^2\Sigma^+$ system were also calculated which were in good agreement with experimental intensities.

d. Radiative lifetime measurement in neutral zirconium and lanthanum atom

Measurements of the radiative lifetimes of the excited atomic levels, combined with branching fractions, provide one of the most reliable methods for determining absolute transition probabilities. In supersonic atomic beam the excitation of atoms takes place in collision-free environment and thus measured radiative lifetimes are free from collisional effects.

We have measured radiative lifetimes of odd parity energy levels of zirconium atom in the energy range 17400–29300 cm^{-1} using time-resolved LIF in supersonic free-jet [12]. The radiative data of spectral lines on rare earth elements is of commercial

importance due to their use as additives in metal halide high-intensity discharge lamps. In neutral lanthanum, we measured radiative lifetimes for 63 odd-parity energy levels, in the range 13260–30965 cm^{-1}[13]. Lifetime values reported in this work fall in the range 10 to 315 ns and are accurate to ±10%.

e. LaO clusters

Transition metal oxide nano particles find applications in electronics, magnetic materials and in catalysis. We produced the metal clusters La_mO_n (m=1-15) for the first time in our laboratory. We have carried out mass spectrometric investigations on these systems and found that cluster oxides for each value of m form only a limited number of stoichiometries; $LaO(La_2O_3)_x$ species are particularly intense (Fig. 5). Threshold photoionization spectroscopy was used to determine the vertical ionization energies of the most abundant species La_3O_4, La_5O_7 and La_7O_{10}. The experimental findings will be combined with *ab initio* quantum chemical calculations for determining their geometric structures.
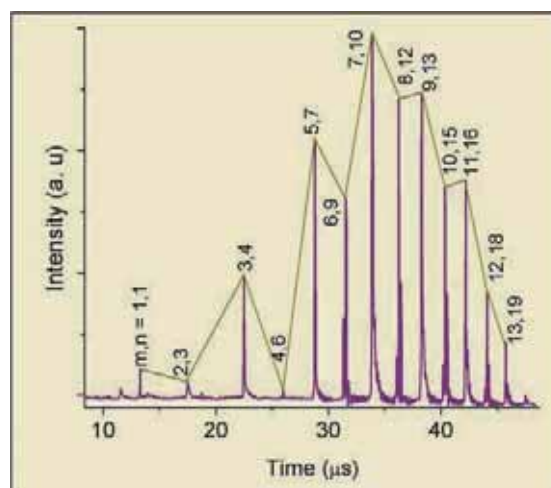
Fig. 5: Time-of-flight mass spectrum of La_mO_n clusters.

Conclusions and future directions

An indigenous laser vaporization supersonic molecular beam experimental setup has been developed within the time frame of 11th plan project. This is the first of its kind in the country. The setup has been utilized to study the electronic structures

of metal-containing diatomic molecules, namely ScN, ScO and LaH. The ground state of these molecules has been assigned unambiguously by our work. We also established the important singlet-triplet energy linkage in LaH molecule. The low energy excited states of these molecules reported by us may stimulate more refined *ab initio* studies, leading to a better understanding of the electronic structure of these molecules. We have initiated studies in metal clusters with mass spectrometric investigations on La_mO_n clusters and are in the process of developing a binary metal cluster experimental setup in the 12th plan to address a wide range of scientific problems in binary metal cluster physics.

Acknowledgement

References

1. Ramsey, N. F., "Molecular Beams" (Clarendon Press, Oxford, U.K., 1956), ISBN 0-19-85 2021-2.

2. Dietz, T. G., Duncan, M. A., Powers, D. E., and Smalley, R. E., "Laser production of supersonic metal cluster beams". *J. Chem. Phys.* 74 (1981) : 6511-6512.

3. Hopkins, J. B., Langridge-Smith, P. R. R., Morse, M. D., and Smalley, R. E., "Supersonic metal cluster beams of refractory metals: Spectral investigations of ultracold Mo_2". *J. Chem. Phys.* 78 (1983) : 1627-1637.

4. Ram, R. S., and Bernath, P. F., "Fourier transform emission spectroscopy of ScN". *J. Chem. Phys.* 96 (1992) : 6344-6347.

5. Chertihin, G. V., Andrews, L., and Bauschlicher, C. W., "Reactions of Laser-Ablated Scandium Atoms with Nitrogen: Matrix Infrared Spectra and DFT Calculations for Scandium Nitrides and the Fixation of Nitrogen by Two Scandium Atoms". *J. Am. Chem. Soc.* 120 (1998) : 3205-3212.

6. Mukund, S., and Nakhate, S.G., "Electronic structure of ScN: Jet-cooled laser-induced fluorescence spectroscopy". *Chemical Physics Letters* 496 (2010) : 243-247.

7. Mukund, S., and Nakhate, S.G., "Jet-cooled laser-induced dispersed fluorescence spectroscopy of ScN: Observation of $a^3\Sigma^+$ state". *Chemical Physics Letters* 501 (2011) : 221-225.

8. Leanhardt, A.E., Bohn, J.L., Loh, H., Maletinsky, P., Meyer, E.R., Sinclair, L.C., Stutz, R.P., and Cornell, E.A., "High-resolution spectroscopy on trapped molecular-ions in rotating electric fields: A new approach for measuring the electron electric dipole moment. *Journal of Molecular Spectroscopy* 270 (2011): 1-25

9. Yarlagadda, Suresh, Mukund, Sheo, and Nakhate, S. G., "Jet-cooled laser-induced fluorescence spectroscopy of LaH: Observation of new excited electronic states'.*Chemical Physics Letters* 537 (2012) : 1-5.

10. Mukund, Sheo, Yarlagadda, Suresh, Bhattacharyya, Soumen, and Nakhate, S. G., "Energy linkage between the singlet and triplet manifolds in LaH, and observation of new low-energy states". *Journal of Chemical Physics* 137 (2012) : 234309.

11. Mukund, Sheo, Yarlagadda, Suresh, Bhattacharyya, Soumen, and Nakhate, S. G., "Jet- cooled laser-induced fluorescence spectroscopy of $B^2\Sigma^+–X^2\Sigma^+$ system of scandium monoxide: Improved molecular constants at equilibrium". *J. Quant. Spectrosc. Radiat. Transfer* 113 (2012) : 2004-8.

12. Nakhate, S. G., Mukund, Sheo and Bhattacharyya, S., "Radiative lifetime measurements in neutral zirconium using time-resolved laser induced fluorescence in supersonic free-jet". *J. Quant. Spectrosc. Radiat. Transfer*, 111 (2010) : 394-8.

13. Yarlagadda, S., Mukund, Sheo and Nakhate, S. G., "Radiative lifetime measurements in neutral lanthanum using time-resolved laser-induced fluorescence spectroscopy in supersonic free-jet". *J. Opt. Soc. Am.* B 28 (2011) : 1928-33.

Xenon Transport in Uranium-10wt% Zirconium Alloy

S. Kolay, A.N. Shirsat, M. (Ali) Basu and D. Das

Chemistry Division

Abstract

The transport kinetics of fission product Xe in U-10wt% Zr alloy matrix was obtained using Post Irradiation Annealing (PIA) technique. From the kinetic data analysis, it was observed that the gas release from the cast microstructure of the irradiated alloy is significantly influenced by grain boundary transport. The transport property derived from this study could be represented as $\ln D'(s^{-1}) = (-13697 \pm 2380)/T - (6.2 \pm 1.8)$, from which the activation energy and frequency factor come out to be 114 kJ.mol^{-1} and 2.03 x10^{-3} s^{-1}, respectively. Presence of the oxygen impurity (<10 ppm) in the carrier gas augmented the transport kinetics.

Introduction

One of the important mandates in the three-stage nuclear power generation programme of India is to utilize uranium-plutonium based alloy fuels in enabling shorter doubling time for breeding of the fissile isotopes ([239]Pu and [233]U) which are used in the thorium based driver fuel in the third stage. For the analysis of high burnup performance the transport characteristics of the fission gases in the alloy matrix should be known. The transporting species and the alloy microstructure both play crucial role in diffusion. The data of bulk and grain boundary diffusion properties of the transporting species in the alloy help in evaluation of gas release behavior and fuel performance.

The cast structure of alloy has less distinguishable grains and their boundaries, and is more prone to disintegration due to the fission gas bubble accumulation. Here, the transport property of gas atom inside grain where it is produced, or, along grain boundaries that are filled with amorphous gel-like [1, 2] phase, will be quite different from that observed in the polycrystalline matrix with distinguishable grain boundaries. The grain and grain boundary diffusions together may play important roles in the overall release rate of gas from the alloy matrix. There are a few reported studies on the diffusion property of Xe in actinide metals like uranium and thorium [3-5] and moreover, Xe diffusion properties in uranium metal as reported in [4, 5] are not consistent.

In this study, carried out at the Chemistry Division, BARC, the kinetic data for the transport and release of xenon in the base alloy, U-10wt%Zr, were obtained using the Post-Irradiation Annealing technique (PIA) of trace-irradiated samples at different temperatures. The PIA technique was also indigenously designed and fabricated.

Experimental

The master alloy (U-10 wt% Zr) was prepared in button form by repeated arc melting of requisite amounts of the two metallic constituents in a water cooled copper hearth, under purified argon flow condition. Nuclear grade uranium of purity 99.5% (200 ppm C, 100 ppm Fe and 200 ppm others (Ca, Mg, Si, Cr, etc.)) was obtained from the Atomic Fuels Division, BARC and crystal bar zirconium was obtained from the Materials Processing Division, BARC. Before the arc melting step, U and Zr metals were treated with dilute HNO$_3$ to remove the oxide layer from the surface, then washed with acetone to get rid of moisture contamination. The prepared alloy was characterized for phase content by XRD (Fig.1), phase morphology by Scanning Electron

Microscopy (SEM), and for compositional homogeneity and oxygen content by chemical analyses. The compositional homogeneity was also checked by EDS. Line widths in the X-ray diffraction pattern were considered to get an idea of crystallite size in the alloy cast. SEM micrographs at different magnifications were noted on a cut section, which were polished and etched for the purpose. Atomic Force Microscopy (AFM) analysis for the surface topography was also carried out particularly for noting the correspondence of the morphology seen in SEM image. For successive studies of xenon release by post irradiation annealing at different temperatures, the master alloy was cut into small pieces (approx. $1 \times 1 \times 2mm$). For each experimental run of the isothermal annealing, three such pieces together weighing about 100 mg were trace irradiated in reactor, in a sealed vial for 4h, maintaining near ambient temperature. The irradiation flux of thermal neutrons, 2.3×10^{15} n m^{-2} s^{-1} was obtained by monitoring ^{198}Au activity (411.8 keV γ, $t_{1/2}$ = 2.7 d) using gold standard. After the required cooling period ($\sim$ 10 days), a known amount of the irradiated sample was isothermally annealed under He gas flowing condition. The released Xe was trapped in liquid N_2 cooled charcoal and the cumulative release was monitored for 81KeV γ-energy of ^{133}Xe ($t_{1/2}$ 5.27 d) by NaI(Tl) detector placed below the charcoal trap. To avoid volatile fission products like iodine and tellurium reaching the charcoal trap, the gas stream from sample passed through a hot copper bed. The schematic of the apparatus is given below (Fig. 2).

Typically, an isothermal release run was carried out for over $\sim$200 min. The initiation of the release kinetics was controlled by instant *in-situ* operation of pushing the sample holder, a platinum boat holding the irradiated alloy chips, inside the hot isothermal zone of a horizontally placed tubular muffle furnace. Helium flow rate was established at 10 ml min^{-1} that ensures complete absorption of the released Xe in the cooled charcoal trap. Before carrying out the experiment, the detector was

Fig. 1: XRD pattern of U-10 wt%Zr (as cast)

Fig. 2: Schematic diagram for PIA study

calibrated by ^{133}Ba source, which is also having 81KeV γ-energy. The isothermal annealing was carried out within a temperature range of 1225K to 1390K with a gap of 15 K. The lower and higher temperature limits were chosen after considering the detector sensitivity and release kinetics, respectively. The furnace temperature was controlled within ±1 K. For these runs, the helium gas was additionally treated for the removal of trace impurities of oxygen, moisture and nitrogen for which the gas was passed successively through the columns of silica gel and hot bed ($\sim$673 K) of uranium turnings. The purifier system was designed to bring down the oxygen partial pressure from 10^{-5} bar (10 ppm) to less than 10^{-15} bar. Some experimental runs were performed without this

additional gas purification step in order to see the effect of oxygen impurities on the Xe release kinetics from the alloy.

The onset of the cumulative release of Xe activity as noted in the monitor was considered as the initial time in the kinetic analysis. To measure the total Xe content in the irradiated alloy, a known amount of the as-irradiated sample was dissolved in dilute HNO_3 containing 7% HF and the released Xe was swept into the liquid N_2 cooled charcoal trap, under the same experimental condition, as was followed during the isothermal annealing study. For the evaluation of fractional release, the total xenon content was appropriately scaled up by taking into account the ^{133}Xe decay that had occurred due to any time lag between the isothermal annealing and dissolution experiments of the alloy. From the observed data of Xe release kinetics at different temperatures, diffusion coefficients of the gas were evaluated.

Results and discussion

The major XRD peaks in Fig.1 correspond to those of (γ-U, γ -Zr) solid solution with a distinct shift from those of pure γ-U phase. The presence of weak intensity lines due to UZr_2 phase are seen in the XRD pattern. The impurity phase, however, could not be identified in SEM analysis of the alloy. The widths of principal peaks at low 2θ values ($<60^0$) corroborate to an average crystallite size of $\sim$ 10 nm. The oxygen content in the sample was found to be less than 0.15 weight%. SEM micrographs at

different magnifications on a cut section of the as-prepared alloy are shown in Fig.3(a), 3(b). The microstructure generally shows martensitic patterns made of disorderly oriented platelets. Atomic force micrograph shown in Fig.3(c) reveals the same characteristics in nanoscale, namely, several platelets of ~100 nm width are grouped together over 500-1000 nm space. The disorder in orientation of the Widmanstatten type platelets is possibly the result of fast freezing through the monotectoid phase field of the alloy (U-10wt% Zr), in the cooled copper hearth during the preparation. On prolonged annealing (~30d) at high temperature under vacuum, the platelets changed over to the regular lamellar form (Fig.4) as reported by other investigators [6,7].
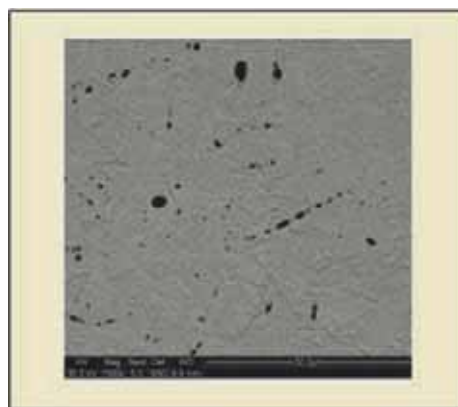
Fig. 4: Annealed (30d, 1273 K) U-10w%Zr (1500x magnification); $<50\mu m$ grains showing lamellar structure
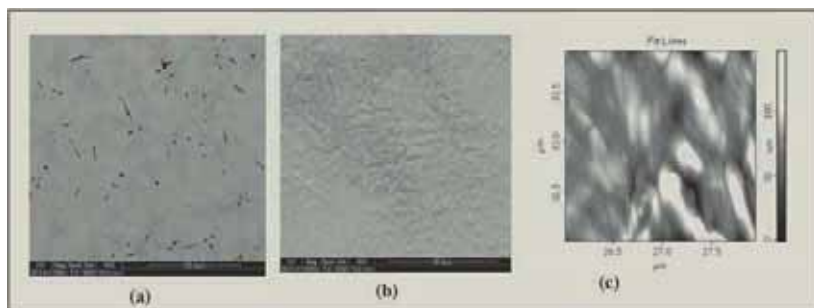
Fig. 3: (a) Microstructure (500x magnification) of U-10w%Zr cast (diffused martensitic pattern, plate-width $>10\ \mu m$) (b) Widmanstatten type platelets ($\geq 1\mu m$) within martensitic plates of U-10w%Zr cast (3000x magnification), (c) AFM picture of U-10wt%Zr cast surface (lamellar colonies within platelets).

At higher annealing temperature, the cumulative fractional release of Xe from the trace-irradiated U-Zr alloy sample showed a uniform parabolic rise, and it points to a regular kinetic mechanism of the gas atom transport inside the alloy. In the functional plot of cumulative fractional release versus √ (time) the regular

behavior is depicted by linear slope as given in Fig 5a. The release plots at lower temperatures, however, exhibit stepwise linearity indicating changeover of the kinetic paths (Fig.5a) in the release.

In contrast to the above stated observation, the Xe release was seen augmented almost thirty times when the carrier gas was used without the additional purification step for its oxygen/nitrogen/moisture impurities (less than 10 ppm). From the release kinetics of the different isothermal annealing runs with the trace irradiated alloy, the transport coefficient of Xe was evaluated for the as prepared alloy matrix in the two situations, namely, the use of carrier gas He (i) with additional purification and (ii) without additional purification. The strikingly different release kinetics with and without purified carrier gas are evident in the two figures, Fig.5a and Fig.5b that respectively describe the two cases. Noting this difference, elaborate studies were made to obtain the transport coefficients at different temperatures for the two cases. The transport coefficient was analyzed from the parabolic part of the cumulative release. For the peculiar case of stepwise parabolic growth of cumulative release as noted only for the case (i) at lower temperatures, the ultimate growth rate was considered in the analysis. The value of diffusion coefficient (D') was derived from the slope of the linear part of fractional release versus √(time) plot with

the consideration of the reported correlation [8,9], $f = 2(S/V)\sqrt{Dt/\pi}$, where f is the cumulatively released fraction over time from a solid sample that has surface area S and volume V. The stated relation derived using Fick's equation is valid for low release ($\leq 25\%$) from the solid material which from a uniform initial concentration distribution of the diffusing species has been subjected to null concentration value at its boundary. For the solid matrix of rectangular parallelepiped (arm lengths, a, b and c) the characteristic dimension can be described by $d = 2 (S/V)^{-1}$, $(1/d = 1/a + 1/b + 1/c)$, and the jump probability by $f = 4\sqrt{D't/\pi}$, $(D' = D/d^2)$, where D' represents the jump frequency of the species over the characteristic dimension d of the matrix. With the sample dimensions of 2mm x 1mm x 1mm, the value works out to be 0.4 mm. D', also called apparent diffusion coefficient of the species, was characterized for Xe in the U-10wt%Zr alloy with cast microstructure (case(i) and case(ii)) at different temperatures. For the steady release part, the transport coefficient shows Arrhenius temperature (T) dependence given by, $D' = D'_0 Exp (-Q/RT)$ where Q is the barrier energy. The plots of D' versus 1/T for the parabolic release of xenon from U-10wt%Zr alloy-cast are shown in Fig. 6. For case (i), the linear least square fitted representation of the data as $\ln D'(s^{-1}) = (-13697 \pm 2380)/T - (6.2 \pm 1.8)$, (12851393), corroborates to the
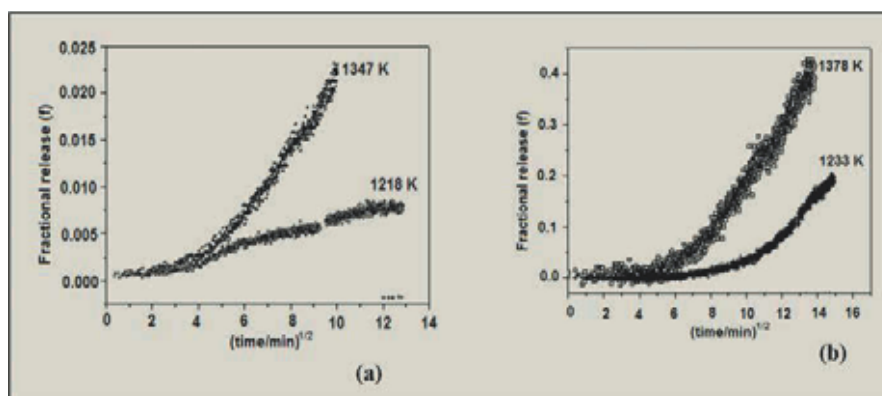

Fig. 5: (a) Xe release kinetics in U-10wt%Zr cast in case (i) (purified helium used for Xe sweeping), (b) Xe release kinetics in U-10wt%Zr cast in case (ii) (unpurified helium used for Xe sweeping)
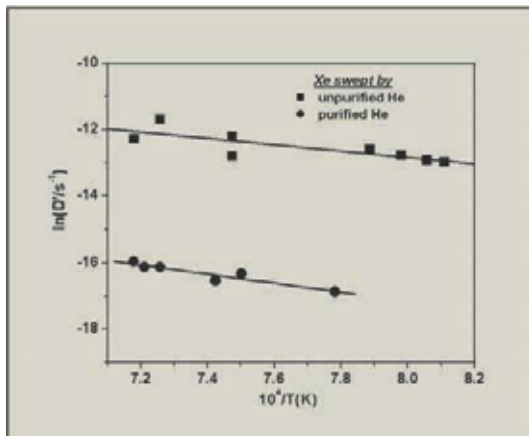
Fig. 6: Arrhenius plot of Xe transport coefficients

activation energy and frequency factor as 114 kJ.mol^{-1} and 2.03 x10^{-3} s^{-1} respectively.

Thus $D_0 \equiv d^2 D_0$ = 3.2 x10^{-10} m^{2}s^{-1}.

The transport regime in the alloy with cast microstructure is evidently different from that in granular structures as reported in the previous studies [3] and [5]. Fission generated fragments like Xe while produced in trace irradiation of the alloy are quite evenly distributed in crystallites as well as their inter spaces, because the fragments have long range (~10 μm) as compared to the dimension of tiny crystallites (~10 nm) constituting the microstructure. The structural insights shown in the 100 μm and 10 μm domains (Fig.3(a), 3(b)) together with the AFM information in the submicron domains (Fig.3(c)), point to the fact that the tiny crystallites constitute the lamellar colonies of Widmanstatten type platelets (≥1 μm width) that in turn constitute a long range order pattern of martensitic plates (>10 μm width). The diffused nature of the martensitic pattern (Fig.3(a)) is indicative of the presence of amorphous [1] or gel-like [2] frozen mass, filling the inter spaces of crystallites. Xe in the inter space region encounters a lower barrier energy in its thermal transport as compared to that in a well developed grain present in annealed state. Here the grain (crystallite) boundary plays predominant role in the composite transport. The amorphous state as compared to the well formed lattice bears higher defect concentration and imparts lower barrier

energy to impurity diffusion. The experimentally arrived barrier energy of 114 kJ mol^{-1} is thus lower than the self diffusion energy of U atom, though it is not as low as that normally expected (50-80 kJ mol^{-1} [2]) for vacancy diffusion along the clearly delineated grains and their boundaries in a polycrystalline solid. In trace irradiated sample, the impediment from gas bubble and fission products precipitate are anyway absent [10] in the grain boundary transport. The high mean square displacement rate (3.2 x10^{-10} m^{2}s^{-1}) as derived in this study again corroborates to the presence of high vacancy concentrations in the inter-crystallite space, high vacancy concentration helps in making successful jumps. The metastable amorphous/gel-like state is chemically more active and it being in the inter space region can easily access oxygen impurity from the carrier gas to undergo crystallite precipitation of oxidized state. The impurity atom and vacancy can make faster mobility during crystallite precipitation, and hence this renders augmented release of impurity atom like Xe. The Arrhenius plot of D' versus 1/T for the steady state part of the parabolic release of xenon in case (ii), where the carrier gas was not purified, is also shown in Fig. 6. The linear least square fitted data represented by ln D'(s^{-1}) = (-9468 ± 2908)/T –(5.3 ± 1.8), (1225≤(T/K)≤1393), corroborates to the activation energy and frequency factor of 79 kJ.mol^{-1} and 5.14 x10^{-3} s^{-1}, respectively. Thus $D_0 \equiv d^2 D_0$ 8.2 x10^{-10} m^{2}s^{-1}.

The barrier energy of 79 kJ mol^{-1} is significantly low as compared to that obtained in case (i) where additionally purified He gas was used. Possibly, the transformation of mucky amorphous deposits to crystallites of oxidized state that is attained through chemisorptive oxygen uptake makes good for the grain boundary passage of low barrier energy for Xe atom. The result of this study thus leads to the following noteworthy point:

High energy impact of fission fragments in the reactor irradiation of fuel pin will invariably result in the continuous presence of smeared amorphous

matters within the polycrystalline alloy matrix. The presence of this kind of phase at high burnup has been reported particularly in the peripheral region of the oxide fuels. Therefore, the Xe transport in such matrix will encounter energy barrier significantly lower than that of U self-diffusion.

Conclusion

This study of Xe release kinetics in trace irradiated U-10wt% Zr alloy having cast microstructure showed, that activation energy in the transport is significantly lower than the self diffusion energy of uranium, but it is quite higher than the grain boundary diffusion energy generally reported for matrices with granular microstructures. The noted nature of the barrier energy is characteristic of the matrices made of tiny crystallites smeared with metastable matters of amorphous or gel like phase present in the cast structure. The noted finding has significance in the simulation analysis of Xe transport and release in the fast breeder alloy fuels.

References

1. Gerhard Wilde (Ed), *Nanostructured materials*, *Amsterdam, Elsevier, 2009.*

2. Yu. P. Valiev, Grain Boundary Diffusion and Properties of Nanostructured Materials, Cambridge, 2007.
    http://www.CISP-publishing.com.

3. C.H. Fox, Jr., C.M. Craft and L.R. Zumwalt, "The diffusion of fission products in thorium metal". *J. Nucl. Mater*. 62(1976):17-25.

4. J.W. Savage, Diffusion of fission gas in uranium, Atomics International Div. of North American Aviation, Inc., Canoga Park, Calif., 1963 August 15, NAA-SR-Imlu.

5. R. Münz, O. Hladik, S.A. Marel, S. EL-Bayoumy, and M. EL-Graphy, "^{133}Xe release during post-irradiation annealing of uranium metal in the presence of a constant volume of air". *J. Radioanal. Chem.* 45(1978): 141-146.

6. C. Basak, G.J. Prasad, H.S. Kamath, and N. Prabhu, "An evaluation of the properties of As-cast U rich U-Zr alloys'. *J. Alloy Compd*., 480(2009):857-862.

7. C. Basak, R. Keswani, G.J. Prasad, H.S. Kamath, N. Prabhu, and S. Banerjee, "Investigation on the martensitic transformation and the associated intermediate phase in U-2 wt%Zr alloy". *J. Nucl. Mater.,* 393(2009):146-152.

8. W. Inthoff and K. E. Zimen, Kinetik der Diffusion radioaktiver Edelgase aus festen Stoffen nach Bestrahlung. Trans. Chalmers Univ. Techn. (Goteborg) 176(1956)16, AEC-tr-3289.

9. T. Lagerwall and K. E. Zimen, Euratom Rept. EUR 1372e (1964).

10. Paul Van Uffelen, Ph.D. Thesis, "Contribution à la modélisation du relâchement des gaz de fission dans le combustible nucléaire des réacteurs à eau légère", Universite de Liège, January 2002.

Diffusion Bonding of Nuclear Materials

K. Bhanumurthy
Scientific Information Resource Division
and
D. Joyson and S. B. Jawale
Centre for Design and Manufacture
and
A. Laik and G.K. Dey
Materials Science Division

Abstract

Diffusion bonding has emerged as a competitive advanced technique in joining similar and dissimilar materials which are difficult to join using the conventional methods. The technique is elaborated with emphasis on the key variables, the mechanisms involved and optimisation of the process parameters.The use of hot isostatic pressing in diffusion bonding of materials is also outlined. Finally, some of the activities related to diffusion bonding carried out in BARC, with relevant details, have been discussed.

Introduction

The technology of joining materials is vital to the growth of various industries such as nuclear, aerospace, automotive, power generation, shipbuilding, oil, petrochemical and process engineering. Progress in the various joining technologies enhances the productivity and quality of joined components. Improving productivity and quality by incorporating cost-effective solutions in the manufacturing processes, also requires innovative developments in joining technologies and processes.

Solid state diffusion bonding is an important advanced technique for joining both similar and dissimilar materials. Solid state joining processes are those which produce coalescence at temperatures below the melting point of the base materials being joined, without formation of liquid phase during the process of joining [1]. These processes involve either the use of deformation, or diffusion and limited deformation to produce high quality joints between both similar and dissimilar materials. Diffusion bonding is one such solid state bonding process which is accomplished by bringing the surfaces to be welded together under moderate pressure and elevated temperature in a controlled atmosphere, so as to effect the coalescence of the surfaces [2, 3].

Diffusion Bonding

Diffusion bonding of materials is a solid state joining technique carried out at a suitable temperature and pressure and is defined as a joining process wherein all the faces to be bonded are held together by a pressure insufficient to cause minimum detectable plastic flow, at a temperature below the melting point of any of the parts, when solid state diffusion causes coalescence of contacting surfaces. The process of diffusion bonding thus requires subjecting the pieces to be joined to high temperature and compressive stress, for a finite time interval, to cause bonding of the faying surfaces without producing macroscopic plastic deformation. The temperature of bonding is usually lower than the fusion temperature but high enough to cause sufficient diffusion at the bonding interface, and the operation can be carried out either in vacuum or in controlled atmosphere. Depending upon the materials being joined, a thin layer of interlayer is often introduced at the joining interface.

Since the bonding is accomplished by diffusion of the materials species across the interface, it is a very suitable technique for joining of dissimilar materials and materials combinations, which are otherwise difficult to join by conventional fusion welding, due to (a) difference in melting points and thermal conductivity, (b) formation of brittle intermetallic compound at the joint interface, and (c) unsatisfactory behaviour in service, for example, poor corrosion resistance. Low pressure at the joining interface and shallow thermal gradients ensure minimum microstructural changes, associated residual stresses and distortions in the parts being joined.

Key Variables of Diffusion Bonding

There are several parameters in the process which needs attention to achieve a sound diffusion bonded joint. The extent of bonding and the manner in which it is achieved is governed both by the properties of materials being joined and the process parameters. The surface conditions, the interlayer materials, the surface, grain boundary and volume-diffusion coefficients, creep properties and yield strength are some examples of the materials properties. The primary process-parameters contributing significantly to the diffusion bonding process are bonding pressure (P), bonding temperature (T) and dwell time (t). Apart from these, initial roughness of the joining surfaces and nature of the interlayer, if used, also play important roles both on the process of diffusion bonding and on the properties of the final joint.

Optimization of Process Parameters

The objective of optimization of the process parameters is to obtain the best possible properties of the diffusion bonded joint which is usually quantified in terms of mechanical strength and leak tightness of the joint. The bonding

temperature usually ranges between $0.5 - 0.7\ T_m$, T_m being the absolute melting point of the most fusible material in the combination. Elevated temperatures aid interdiffusion of atoms across the interface of the joint and also assist in surface modification by elimination of asperities. The bonding pressure should ensure tight contact between the edges of the pieces, and must be sufficient to aid deformation of surface asperities and to fill all the voids at the interface by material flow. In case of insufficient pressure, some of the voids may be left unfilled, thus impairing the strength of the joint. Importantly, the compressive load also helps in dispersing surface oxide films. This leaves a clean surface and aids diffusion and coalescence at the interface. When dissimilar metals are to be joined, the choice of the bonding pressure is decided by the mechanical strength of the weaker of the two materials. The dwell time (t), at a specified bonding temperature and pressure must, in most cases, be kept to a minimum from physical and economical considerations. It should be sufficient for an intimate contact to be formed by elimination of the asperities at the interface through the process of solid state diffusion. However, an excessive diffusion time might lead to formation of Kirkendall voids in the weld zone or even change the chemical composition of the metal or lead to the formation of brittle intermetallic compounds
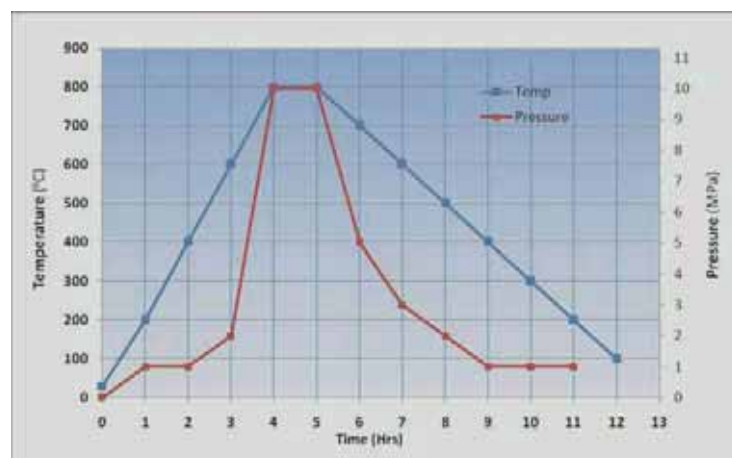

Fig. 1: A typical temperature and pressure cycle during diffusion bonding for bonding copper and stainless steels

(when dissimilar metals are being joined). Fig. 1 shows a typical temperature and pressure cycle in the process of diffusion bonding of Cu/stainless steel system.

Mechanism of Diffusion Bonding

The entire process of diffusion bonding is essentially accomplished in different stages. The changes that take place at the joining interface in each of these stages can be listed as below [4]:

Stage A: Initial asperity or point contact

Stage B: Plastic deformation of the asperities; contact areas increase until the local stresses decrease to below the yield stress

Stage C: Removal of large, irregularly shaped voids at the interface as well as a simultaneous migration of the interfaces out of planar orientation and away from the voids

Stage D: Elimination of the remaining isolated voids by diffusion

Stage E: Grain boundary rearrangement and volume diffusion.

Influence of the Process Parameters on the Stages of Diffusion Bonding

(a) Pressure

Compressive pressure is required during Stage B, to achieve a large area of contact by localised plastic deformation of asperities on nominally flat surfaces. Where appropriate, pressure is also used to bring about the creep mechanisms which contribute to bonding. The applied pressure (*P*) however, must not be so high as to cause macroscopic deformation of the components, as stated earlier, and hence is limited to the yield stress (σ_{ys}). P < σ_{ys} (1)

(b) Temperature

Plastic deformation, creep and the various diffusion mechanisms are all temperature dependent. Temperature determines: (a) the extent of contact area which dictates the size of voids to be eliminated during Stage B, (b) the rate of diffusion which governs void elimination during Stages C, D, and E. Since solid state diffusion is a thermally activated process, the temperature dependence of the diffusion coefficient (D) is given by:

$$D = D_0 \exp(-Q/RT) \qquad (2)$$

where, D_0 and Q are pre-exponential factor and activation energy, respectively.

(c) Dwell time

The creep and diffusion mechanisms are time dependent. Hence, sufficient time must be allowed for void closure by material transfer. Bonding time is affected by temperature, the materials and specimen size. Therefore, the time and temperature for each case should be optimized. The width of the interdiffusion zone (*X*) formed at the interface between the two materials during diffusion bonding is given by:

$$X = k\sqrt{t} \qquad (3)$$

where, *k* is the kinetic rate constant at the temperature (*T*) of bonding and *t* is duration of bonding.

(d) Surface roughness

The grade of surface roughness determines the extent of initial surface contact and the size of voids. This in turn, influences the bonding rate. Surfaces may be prepared by machining, grinding and polishing. In general, a finish better than approximately 0.4 µm is necessary to ensure good initial contact. The removal of surface contaminants and thick oxides prior to bonding is also crucial.

(e) Interlayer materials

Interlayer materials are very useful when bonding dissimilar materials. They serve to reduce temperature and/or pressure required for bonding and also prevent the formation of intermetallic compounds. Soft interlayer materials enhance contact and accommodate the residual stress developed at the interface of dissimilar materials due to the thermal expansion mismatch.

Therefore, it is evident that the process and materials variables are interrelated and will affect the relative contributions to bonding from each of the possible bonding mechanisms.

Diffusion Bonding using Hot Isostatic Pressing (HIP)

Hot Isostatic Pressing or HIP, as it is commonly known, is a materials processing technique which involves uniformly heating up the work-load while an inert gas pressure is applied on its surface. The process is used to fabricate components from materials which are difficult or impossible to form by other techniques. It is also commonly used to consolidate fabricated components such as densifying porous materials and healing internal defects. Powder metallurgy, ceramics and casting are three main applications of HIP [5–8]. However, it is also claimed that diffusion bonding was the original application of HIP [9]. When joining jobs with complex geometries and those involving powders, diffusion bonding process is often considered as the best method of joining. In such cases, the multi-directional application of pressure is needed and hence an isostatic press is considered ideal. As the HIP machine can provide high temperature and isostatic pressure simultaneously, even sintering and diffusion bonding of ceramic powder onto a bulk surface can be carried out at the same time, thereby reducing the processing time.

A typical HIP unit operates from 500 °C to 2200 °C with pressures ranging from vacuum to 210 MPa. It generally consists of a pressure vessel, furnace, gas system, power supply, instrumentation and controls and auxiliary systems. Presently, the technique of HIP diffusion bonding is being used largely in joining metals to themselves, ceramics and composites. Successful joints of ceramics such as the carbides (WC, TiC, TaC) and nitrides (Si_3N_4, TiN, AlN) with metals and alloy like steels, stainless steels, and Ni-based superalloys has been demonstrated using HIP. Development is being made in achieving higher quality bonds in larger numbers of ceramic-metal combinations which can be bonded using HIP.

Interdiffusion and Diffusion Bonding Work at BARC

Diffusion bonding can be employed to effectively to join different combinations of materials. Fig. 2 shows the combination of different materials which are amenable to diffusion bonding with or without using interlayers and the work done at BARC. The presence of a low strength intermediate layer is often used to reduce the temperature and/or pressure required for welding. This ductile inter-layer acts as a stress-relieving structure and hence reduces the accumulated residual stresses in regions around the interface. Interlayers are also required in some dissimilar metal systems to prevent the formation of brittle intermetallic phases in the weld. Therefore, understanding of the interdiffusion behaviour of various materials combinations assume significant importance in selection of interlayer. Detailed investigations were carried out to study the diffusion reactions and evaluate the interdiffusion characteristics of various systems such as Zr-Al [10], Zr-Ti [11], Cu-Ti [12], Ni-Al_2O_3 [13], Mo-Ti [14] and
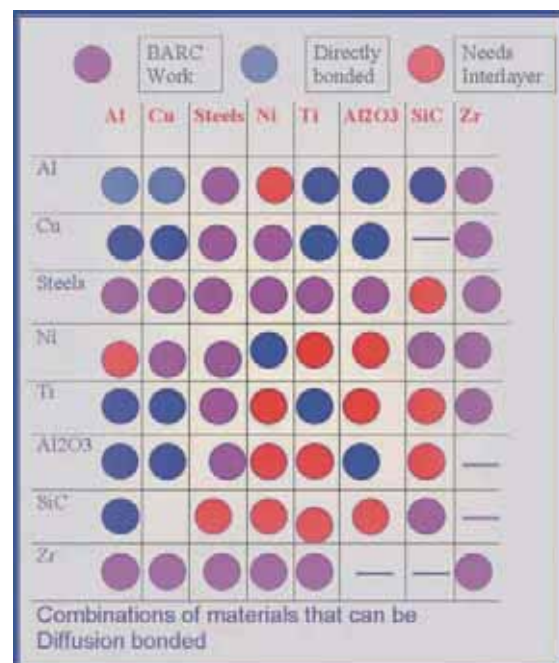

Fig. 2: Combinations of different materials those are amenable to diffusion bonding, with and without interlayers. The combinations which were bonded in BARC are identified by pink dots.

zircaloy 2- Inconel [15]. In fact some of the diffusion coefficients were used for optimising the diffusion bonding parameters [16].

On the other hand, diffusion bonding requires a substantially longer joining time. In addition, the equipment costs are high due to the combination of high temperature and pressure in vacuum environments.

Work Related to Diffusion Bonding of Materials in BARC

Diffusion bonding technique has been successfully used to join a variety of material combinations and a few of them are discussed below.

(a) Diffusion bonding of aluminium to stainless steel

Joining of Al and its alloys to SS 304 is frequently required in cryogenic and nuclear applications. A variety of aluminium alloys are used as storage tanks for cryogenic liquids and transfer links are mostly stainless steel connectors. This requires a transient joint between these two alloys. Such joints find wide applications in the development of neutron-sensitive ion chamber and proportional counter for reactor control and safety instruments. These joints are also used in the development of ion chamber for environmental monitoring of low energy gamma rays and X rays.

The most common methods employed for joining Al alloys to SS are brazing, friction welding, explosion welding and solid state diffusion bonding. Welding and brazing of these alloys are difficult due to large differences in their melting points, thermal expansion coefficients and thermal conductivities. Besides, formation of brittle intermetallic compounds at reaction zone may lead to premature failure of the joint. Friction and explosion welding joints generally result in the development of large residual

stress and structural discontinuity at interface. Diffusion bonding offers sound strength and high leak-tight joint when silver interlayer was used. Successful Al/SS joints were prepared by diffusion bonding at 300 °C for 2h and pressure about 10 MPa, using various interlayers of Zn, Cu, Ag on the Al side and Ni, Cu, Ag on the SS side [17]. Fig. 3(a) shows joint assembly for use in neutron counters. The microstructure of the interface of cross-section of the SS/Al joint is shown in Fig. 3(b).

(b) Manufacturing of perforated plate matrix heat exchanger for cryogenic application

Perforated plate matrix heat exchanger is a compact and highly effective heat exchanger for liquifying of helium in cryogenic application. The heat exchanger essentially consists of a stack of perforated copper plates alternating with stainless steel (SS) spacers. The diffusion bonded joint between Cu/SS has been developed, to fabricate a cryogenic matrix heat exchanger. Stacks consisting of plates and spacers (75 each) and two stainless steel end plates were bonded to form monolithic heat exchanger, as shown in Fig. 4(a). A typical micrograph of the SS/Cu interface is shown in Fig. 4(b). Special fixture was fabricated to hold the stack of Cu sheets, SS spacers and the end plates. The process parameters were optimized and the heat exchangers were successfully manufactured, meeting the required properties.
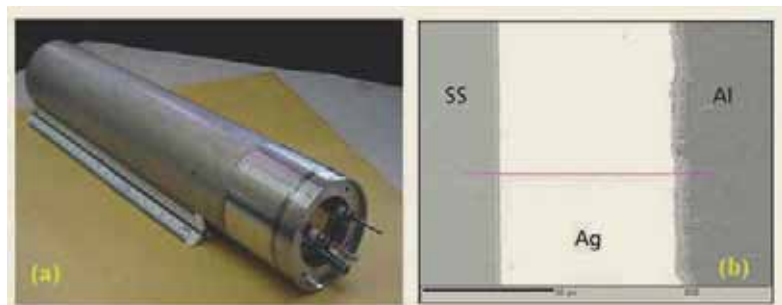

Fig. 3: (a) Stainless steel / aluminium joint assembly diffusion bonded with interlayers at 350 °C for 2 h used in neutron counters (b) micrograph showing the transition interface between the two base materials, the pink line shows the regions where EPMA was done.
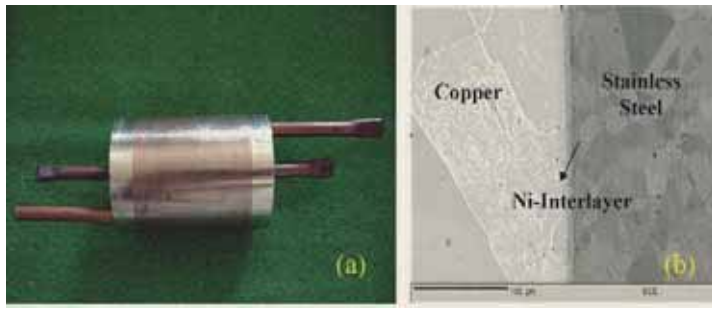
Fig. 4: (a) Alternate layers of Cu plates and stainless steel spacers along with two end plates diffusion bonded to form a matrix heat exchanger for cryogenic applications, (b) backscattered electron micrograph of the copper-stainless steel interface showing good bonding throughout.

(c) Zircaloy-2/stainless steel joints

Many irradiation experiments are carried out in pressurised water loop system in research reactors, to evaluate the design parameters and their effects on the fuel performance. In-pile instrumentation probes are used, for measuring parameters such as temperature and pressure. The joining of Zircaloy-2 (Zr-2) and SS by conventional welding, leads to the formation of brittle intermetallic compounds such as $FeZr_2$ and FeZr, in the weld pool which impairs the strength of the joint. Further, because of large variation in thermal expansion coefficient and elastic modulii high residual stress develops during cooling of weld leading to failure of the joint. Transient joints

between Zr-2 and SS-304 required for in-pile instrumentation in nuclear reactors were made using interlayers of Nb, Cu, Ni and diffusion bonded in solid state at 900 °C for 2 h at 15 MPa stress. The strength of joint is around 300 to 450 MPa and the joint has negligible leak rate. The joints were successfully tested to withstand thermal cycling of 30 cycles from 300 °C to room temperature with reduction in strength only by 10%. Zr-2/SS joint has also been made by the transient eutectic bonding technique.

(d) Diffusion bonding of stainless steel to titanium

Joining of SS to Ti is required in nuclear and chemical engineering applications. Apart from having good strength, such joints need to possess stringent leak tightness and corrosion resistance to aggressive corrosive fluids. SS and Ti substrates were bonded directly as well as by using suitable interlayers in vacuum at temperatures in the range 800 – 1000 °C and pressure of 10-20 MPa for a dwell time between 30 min and 2 h. Although a bond strength of about 90% of the strength of the parent materials was achieved using multi layers of foil at the

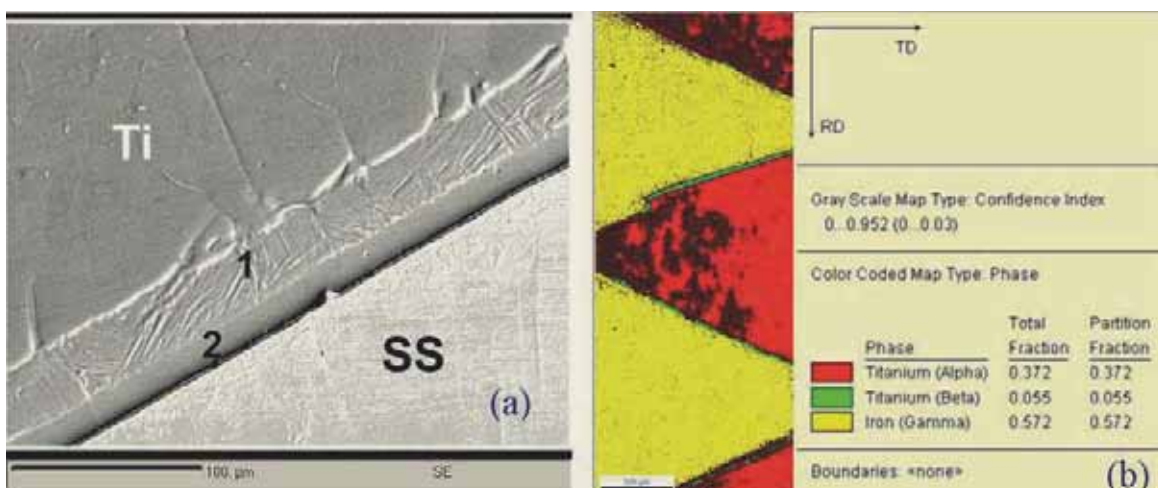Fig. 5: (a) Electron micrograph of cross section of Titanium-Stainless Steel diffusion bonded joint, Layer 1: α-Ti needles in β-Ti matrix, Layer 2: β-Ti (Fe, Ni, Cr). (b) EBSD phase maps showing formation of a layer of β-Ti layer at the interface.

interface, such joints were susceptible to degradation in nitric acid environment. Hence direct bonding was optimized for specific applications where good leak tightness and adequate corrosion resistance were achieved. Fig. 5(a) shows a typical microstructure of the cross-section of SS/Ti diffusion bonded interface. The phase maps shown in Fig. 5(b) delineated the formation of a layer of β-Ti in the joint interface due to interdiffusion.

Summary

Diffusion bonding is a versatile technique for bonding metallic materials and has been extensively used for joining both similar and dissimilar materials at BARC. Special mention should be made related to joining of stainless steels to aluminium alloys, copper and titanium for fabricating end products of direct relevance to DAE programmes.

References

1. N. F. Kazakov, Diffusion Bonding of Materials, Pergamon Press (1985).

2. P. M. Bartle, Diffusion bonding as a production process – Information Package Series, The Welding Institute, Cambridge, p. 1, (1979).

3. P. G. Partridge, and C.M. Ward-Close, *Metals and Materials*, Vol.5, p. 334 (1989).

4. M.G. Nicholas, Design interfaces for technological applications: ceramic-ceramic, ceramic-metal joining, Eds. S.D. Peteves, *Elsevier Applied Science*, p. 48 (1989).

5. L. Buekenhout and P. Alt, *Key Engineering Materials*, Vol.29-31, p. 207 (1989).

6. O. Yeheskel, Y. Gefen and M. Talianker, *Proceedings of the 3rd International Conference on Isostatic Pressing*, Vol. 1, Paper 20 (1986).

7. E. L. Rooy, *Modern Casting*, p. 18 (1983).

8. R.A. Stevens, P.E.J. Flewitt, *Materials in Engineering*, Vol.3, p. 461 (1982).

9. Zimmerman, EX., and W.H. Walker, *Proceedings of the 2nd International Conference on Isostatic Pressing*, Vol. 2, paper 22 (1982).

10. A. Laik, K. Bhanumurthy, G.B. Kale, *Intermetallics*, Vol. 12 pp. 69-74 (2004).

11. K. Bhanumurthy, A. Laik, G. B. Kale, *Defect and Diffusion Forum*, Vol. 279, pp. 53-62 (2008).

12. A Laik, K. Bhanumurthy, G. B. Kale, B. P. Kashyap, *International Journal for Materials Research*, Vol. 103, pp. 661-672 (2012) .

13. A. Laik, D.P. Chakravarthy, G.B. Kale, *Materials Characterization*, Vol. 55, pp. 118-126 (2005).

14. A. Laik, G.B. Kale and K. Bhanumurthy, *Metallurgical and Materials Transactions* A, Vol. 37A, pp. 2919-1926 (2006).

15. A. Laik, P.S. Gawde, G. B. Kale, K. Bhanumurthy, *Materials Science and Technology*, Vol. 25, pp. 1453-1457 (2009).

16. S. Kundu, M. Ghosh, A. Laik, K. Bhanumurthy, G. B. Kale and S. Chatterjee, *Materials Science and Engineering* A, Vol. 407, pp. 154-160 (2005).

17. K.Bhanumurthy, G.B.Kale, S.Banerjee, J.Krishnan, D.Derose, A.L.Papachan and A.K.Grover, Solid state diffusion bonding of aluminium alloys to stainless steel. (Patent No. 24151,643/MUM/02 dated 12 July 2002.

Microwave Processing in Thorium Fuel Cycle

G.K. Mallik
Post Irradiation Examination Division

Abstract

Thorium fuel cycle requires innovative, remote controlled and maintenance-free technologies due to the presence of ^{232}U and other hard γ-emitting isotopes with its main fissile constituent ^{233}U. Microwave heating, due to interaction - absorption and volumetric in nature is material specific. It has an effect on the process and the quality of the product as well. Use of microwave heating has shown promising outcomes for many processing steps like dissolution, concentration, denitration, calcination, reduction, drying, dewaxing, sintering, incineration, pyrohydrolysis and vitrification in thorium fuel cycle. Microwave applicators can be adapted for use in glove-boxes and hot-cells. This paper presents an overview of the application of microwave heating in thorium based fuel cycle.

Introduction

The success of India's nuclear energy programme depends on the utilisation of its rich thorium resources. The natural fertile ^{232}Th isotope, when used in a nuclear reactor, converts to the fissile ^{233}U isotope by neutron absorption and subsequent radioactive decays. Thorium can be used as a nuclear fuel only after the first cycle of irradiation in a reactor and reprocessing to separate the fissile isotope of uranium. Thorium is generally used in the oxide form, either as thorium dioxide or as a mixed oxide either with uranium or plutonium. Thorium based closed fuel cycle consists of fuel feed preparation, fuel fabrication, irradiation in a reactor, reprocessing of spent fuel and waste treatment. Thorium dioxide being inert is difficult to dissolve[1, 2]. Thorium fuel cycle gets further complicated due to the presence of ^{232}U and other hard γ-emitting isotopes along with reprocessed fissile ^{233}U isotope[3]. The shielding requirement increases with ^{232}U content. Hence, either separation of ^{232}U or use of remote handling techniques in a shielded facility becomes mandatory for fabrication of ^{233}U based fuels.

During conventional heating, only molecules on the surface of the object being heated receive heat from the source directly and then the heat propagates towards the central region, creating a temperature gradient from outer surface towards the centre.

During microwave heating, direct participation of every molecule of the object for heat production, leads to rapid generation of heat in the entire volume of the object and reverses the temperature gradient in contrast with conventional heating[4]. Microwave heating is material specific and not all materials are amenable to microwave heating, as interaction and absorption of microwaves by selective species having polarity or polarisability are essential requirements.

Since most of the equipment to be used for processing of thoria based mixed oxide (MOX) fuel is essentially to be housed in a glove box, their size and ease of maintenance are the governing factors. Use of microwave heating allows remote placement of equipment enabling the optimisation of the size and volume of the processing equipment from the consideration of criticality, reduced waste, effective use of glove box space and so on.

Scope of microwave heating in thorium fuel cycle

Microwave heating can be effectively used in the aqueous processing steps since water molecule is a good absorber of microwave. The endothermic nature of the aqueous process along with low pressure dissolution of ceramic oxides, concentration of liquids, denitration of nitrate solutions resulting

in solid oxide powders and amenability for liquid waste treatment, are the processes where microwave heating can offer advantages. The microwave gelation would eliminate the generation of liquid wastes prevalent in the conventional sol-gel route and can be one of the important techniques for preparation of free flowing microspheres. This will reduce the dust loads and provide free flowing feed for nuclear fuel fabrication.

Extremely high absorption of microwaves by oxides of uranium and plutonium, enhances the scope of solid materials processing in thoria based mixed oxide fuel fabrication during calcination, reduction, drying, dewaxing and sintering. The distinct benefit of microwave heating is during sintering, a vital step in the fuel fabrication flow-sheet. Microwave sintering will improve the quality of fuel pellets and bring down the rejection rate. The microwave sintering can also be used for recovery of rejects, chemical analyses during fuel fabrication and solid waste treatment. Another attractive feature in microwave heating is the adaptability of the same oven for a number of processes and hence, it may be utilised as "*mono-equipment multi-process technique*".

Applications

Dissolution

Microwave heating technique has been efficiently used for the dissolution of sintered ThO_2 and $(Th,U)O_2$ pellets[1, 2]. The use of fluoride ion is necessary in case of microwave dissolution also but nearly half the quantity required as compared to the conventional processes (refluxing). The dissolution rate of sintered pellets at a pressure above 40 psi (0.28 MPa) using microwave heating is one to five orders of magnitude higher than that of conventional heating. The microwave aided dissolution of sintered fresh and scrap fuel pellets up to 0.5-1.0 kg per batch has been established. The use of this technique in the dissolution of thoria based spent fuels can speed up the process. Microwave dissolution of ash, obtained by

incineration of tissue papers and absorption sheets, in a mixture of equal concentrations of nitric and sulphuric acid in pressure vessels has been successfully carried out and can be employed for combustible waste treatment[5].

Concentration and Denitration

Concentration of aqueous/acidic solution is possible as water and acids are good absorbers of microwaves. An important application of microwave heating lies in the preparation of ceramic grade powders of ThO_2, $(Th,^{233}U)O_x$ or $(Th,Pu)O_2$ by a single step microwave denitration /co-denitration of respective nitrate solutions via concentration of solution and solid oxide conversion. The purity of nitrate solutions will be an essential prerequisite for such a process. Thorium and thorium-uranyl nitrate solutions of 1-1.5 litre batches containing 400-450 g heavy metal/litre have been denitrated within 2-3 hrs with provision for condensing and scrubbing the off gases. The advantages of microwave denitration include:

(i)   The processing route embeds non-proliferation aspects of fissile component.

(ii) Powder characteristics improve with regard to particle size, surface area, density and sinterability in comparison to conventional thermal denitration route. Severe grinding of oxide products, like in conventional denitration, is not required.

(iii) Th/U losses and liquid waste generated are negligible.

(iv) Condensed nitric acid is reusable for 2-3 cycles.

(v) ThO_2 powder, prepared using microwave denitration of thorium nitrate solution mixed with Poly Vinyl Alcohol, dissolves in nitric acid without addition of hydrofluoric acid.

(vi) Amenable for continuous process designs.

Gelation (Microsphere Preparation)

Gelation is an alternative and superior route for the preparation of microspheres as free flowing feed for fuel fabrication, specially for $^{233}UO_2$ having $^{232}UO_2$, instead of powder(s) prepared from nitrate solutions either by conventional denitration or

precipitation route. Conventional sol-gel route, using hot silicon oil as gelation medium, generates a large quantity of liquid waste whereas microwave gelation would eliminate it. A microwave gelation system is under testing at PIED.

Calcination / Reduction

Microwave calcination and reduction of 500g of crushed $(Th_{0.9625},Nat-U_{0.0375})O_2$ pellet have been carried out in open and closed quartz vessels, respectively, up to 700°C. UO_2 constituent of the mixed oxide gets oxidised to U_3O_8. During reduction process, UO_3 and U_3O_8 convert to UO_2.

The major constituents of the ceramic waste form SYNROC (oxides of Al, Zr, Ca and Ba) are microwave inactive or poorly active but some constituents like oxides of transition metal of High Level Waste (HLW) are microwave active[6]. Thus microwave calcination of titanate based SYNROC has been successful. Single stage microwave calcination of a mix of SYNROC and HLW constituents involving dehydration, denitration and oxide formation under controlled reducing atmosphere takes place at a faster rate than that of the conventional route and yield products with good homogeneity.

Drying and Dewaxing

Microwave heats the material volumetrically and, hence, the moisture or organic binders even from the core of pellets/powder can be driven out more effectively and rapidly than the conventional methods. There is an appreciable decrease in the H and C contents in $(Th_{0.9625},Nat-U_{0.0375})O_2$ pellets after microwave drying and dewaxing, as compared to that resulting from the conventional route.

Sintering

Microwave sintering works[7,8] on UO_2 reports either the use of a single mode cavity (useful only for 1-2 pellets) or indirectly apply the microwaves (by covering the target pellets with U-oxide powder/sintered pellets) in multi-mode cavity. These schemes are not practically attractive for sintering of a large amount of fuel. Initial studies have established that ThO_2 is a microwave inactive material whereas UO_2

is strongly microwave active. Consequently, direct microwave sintering (i.e. without covering with microwave absorbers) of $(Th,U)O_2$ pellets in an oxidative medium in bulk has been carried out successfully[9] in a multi-mode cavity. Using the high rate of rise of temperature and its sustenance by direct coupling of microwaves, $(Th_{0.9625},Nat-U_{0.0375})O_2$ pellets ($\sim$1.5 kgs per batch) have been directly microwave sintered at $\sim$1300-1350°C in an oxidative medium. The rate of temperature rise is fast but considering the thermal shock, the rate of rise is limited to 2-3°C per minute. A batch of green pellets with green density of 61-63% theoretical density (T.D) was sintered to a density of 91-92% of T.D., without any surface defects.

Scrap Recovery

Two types of scraps are generated during thorium dioxide based fuel fabrication, namely, Clean Rejected Oxide (CRO) and Dirty Rejected Oxide (DRO). CRO consists mainly of pellets rejected during the check for their physical integrity and is mostly a pure feed material in a non-useable form. DRO is in the form of sludge and contains some impurities, since it is generated during the wet centreless grinding of pellets for their dimensional control after sintering. Presently, DRO does not contain significant metallic impurities due to the use of diamond grinding wheels. It does not require any specific purification step. Hence, microwave dissolution and denitration process is sufficient to recycle the scrap.

Incineration, pyrolysis and pyrohydrolysis of α - active combustible waste

Solid α-active nuclear waste, generated during processing of Pu and [233]U based materials, consists of Polyvinyl Chloride (PVC) sheets/bags, cotton, tissue papers and absorption sheets. Microwave incineration of non-chlorinated combustible waste to ash at 600-700°C (to reduce the waste volume by three orders of magnitude in weight and two orders in volume) followed by dissolution of the resultant ash (to recover U/Th) has been successfully carried out. The soot from incineration of waste is mostly contained within the cover and off-gases

are routed through a scrubber. PVC, a chlorinated combustible waste, does not degrade easily and its disposal, especially, when it is á-active, poses serious problems. Incineration of PVC is considered as an option to reduce the waste volume but associated evolution of HCl and toxic dioxin is hazardous[10]. Controlled pyrolysis and pyrohydrolysis of PVC at 400°C under inert gas medium selectively release all chlorine whereas incineration with oxygen gas at 900°C drives out all the carbon present in PVC. Microwave pyrohydrolysis followed by microwave incineration[11] has been successfully applied to ~20 g sample of PVC pieces simulated with 2 g of sintered $(Th,U)O_2$ powder. The residue is 2.4 to 2.5 g, which is dissolved in concentrated nitric acid and 0.5 M hydrofluoric acid mixture to recover all Th and U.

Vitrification

The liquefying temperatures of various waste and precursor glass feed materials with different constituent composition applicable for high level waste vitrification have been verified for 500 g of each with direct microwave heating and are as follows:

Waste Feed (25%) :

$NaNO_3$-(36.2%), $Fe(NO_3)_3$-(9.5%), $NaNO_3$-(0.54%), KNO_3-(0.59%), CrO_3-(0.23%), $Mn(NO_3)_2$-(46.2%), $Sr(NO_3)_2$-(0.1%), $Ba(NO_3)_2$-(0.12%), $Al(NO_3)_3$-(1.9%), $La(NO_3)_3$-(0.2%), $Ce(NO_3)_3$-(0.5%), $Pr(NO_3)_3$-(0.07%), $Nd(NO_3)_3$-(0.4%), $Sm(NO_3)_3$-(0.2%), $Y(NO_3)_3$-(0.2%)

(Strong Microwave Absorber – Liquefies in 5 minutes – 650°C)

Precursor Feed (75%) :

1. Glass Slurry Feed for Induction – Melter :

SiO_2-(40%), H_3BO_3-(13.3%), $NaNO_3$-(25.3%), TiO_2-(7.36%) and MnO-(14%)

(Moderate Microwave Absorber – Liquefies in 20 minutes – 300°C)

2. Glass Frit Feed for Joule – Melter :

SiO_2-(45%), B_2O_3-(27.7%), Na_2O-(12.3%), TiO_2-(10%) and Fe_2O_3-(5%)

(Moderate Microwave Absorber – Liquefies in 30 minutes – 700°C)

The microwave interaction and absorption studies show that microwave vitrification process can be applied with better results than the processes using induction or Joule melters.

Microwave Heating Systems (MHS)

Sturdy, good quality, automated and indigenously developed MHS are necessarily required for the development of the microwave processing techniques. In view of this, indigenous glove-box and hot-cell adaptable MHS (up to 6 kW) have been developed (Figs. 1 & 2) with appropriate applicators.

The rectangular and cylindrical stainless steel microwave cavities and wave-guides (parts inside glove-box/hot-cell) hardly require any maintenance. The power supply-cum-control unit and the tuners have all indigenous components. A microwave transparent but air leak tight window is used at the glove-box/hot-cell interface. A synchronous motor used for the mode stirrer of microwaves is the only component inside the glove-box/hot-cell which needs to be maintained. All quartz, PTFE Teflon, HDPE and alumina vessels are indigenously procured. Magnetron, isolator, power couplers and PFA Teflon made pressure vessels for dissolution work are imported.

Fig.1: Microwave Heating System adapted inside Glove-Box

Fig. 2: Microwave Heating System adapted inside Hot-Cell

Conclusions

It can be concluded that microwave heating techniques can play important roles at various stages in the chemical processing of ThO_2 and its mixed oxide fuel feed preparation, fabrication, scrap recovery and waste treatment. The stainless steel cylindrical microwave cavity (tank) can help in the pressurized (upto 40 psi) microwave dissolution of ThO_2 and its mixed oxide fuels. Microwave denitration of solutions to oxide powders or gelation of nitrate solutions directly to microspheres can provide direct feed for fuel fabrication. The direct microwave sintering technique for $(Th,U)O_2$ and $(Th,Pu)O_2$ would significantly improve the quality of products as well as reduce the maintenance work inside the glove-box and hot-cell. The applications of microwave in radioactive waste treatment stream hold good promise. The most important aspects of microwave heating system are the proper design of cavities, remote controlled operations and adaptation to the isolated / shielded facilities to reduce the tedious maintenance and down-time of equipment, specially for Pu and ^{233}U / ^{232}U bearing materials. The current experience gained during fabricating and adapting the high wattage microwave heating systems for glove- box and hot-cell have added to the indigenisation goals.

References

1. G. K. Mallik et al., NUCAR-92, p155, Dec-1992, Andhra University, Vishakhapatnam, India

2. G. K. Mallik et al., NUCAR -2001, p260, Feb-2001, Pune University, Pune, India

3. Taylor and Francis, Science & Global Security, Vol. 9, p1-32, 2001

4. Willard H. Sutton, *Ceramic Bulletin*, 68(2), p376-386, 1989

5. G. K. Mallik et al., NUCAR-95, p268, Feb-1995, IGCAR, Kalpakkam, India

6. R.D. Ambashta et al., *1st DAE-BRNS symposium on Materials Chemistry*, Dec-2006, BARC, Mumbai, India

7. Chang Young Joung, et al., KAERI, South Korea – Personal Communication

8. T. Subramaniam, et al., *Materials letters* 46 (2000) 120-124

9. G. K. Mallik et al., 2nd DAE-BRNS symposium on Materials Chemistry, Dec-2008, BARC, Mumbai, India

10. Ron Zevenhoven and Loay Saeed in proceedings of R'2000 World Congress on Recovery, Recycling, Reintegration, June 2000, Toronto, Canada

11. G. K. Mallik et al., NUCAR-2009, p143, Jan-2009, SVKM's Mithibai College, Vile Parle, Mumbai, India.

Emergent Biofilm Control Strategies Based on Controlled Release of Antimicrobials: Potential Industrial and Biomedical Applications

Rachna Dave, Hiren Joshi and Vayalam P. Venugopalan

Water and Steam Chemistry Division, BARC Facilities, Kalpakkam

Abstract

Bacterial biofilms are a major cause of concern not only in industrial environments but also in biomedical settings. Prosthetic devices, catheters and shunts placed inside human body are prone to bacterial colonization, leading to biofilm formation. Biofilm control in industrial and biomedical settings share certain commonalities. Provision of inimical concentrations of antimicrobials in the close proximity of the surface to be protected (with the bulk fluid being largely spared) is a desirable strategy. Accordingly, we have developed an antibiotic-enzyme loaded polymer composite, nitrogen oxides releasing wound dressings and a biocide releasing polymer capable of controlled release of antimicrobials for effectively curtailing biofilm growth. Interestingly, this work has emerged as an offshoot of our mainstream work on biofilm/biofouling control in cooling water systems.

Introduction

Biofilms represent a form of surface-attached microbial growth, stabilized in an extracellular polymer matrix secreted by the constituent organisms[1]. Bacterial biofilms are ubiquitous in nature and are formed whenever a non-sterile fluid contacts any solid surface. They can occur on different surfaces like metals, alloys, plastics, glass and natural materials like rocks or human teeth. Industrial systems are particularly at risk as biofilms impact their normal operation and, in many cases, cause deterioration of the substratum material. Enormous amounts of money are spent on controlling this menace in various industrial environments[2]. In the case of human infections, biofilm control requires administration of high doses of antibiotic, as the bacteria ensconced in a biofilm matrix are generally resistant and not eradicated by the regular doses.

The Water and Steam Chemistry Division, Kalpakkam, has been carrying out R&D work on the problem of biofouling in the cooling water systems of power plants with emphasis on development of environmentally sustainable fouling control methods. Conventionally, bulk chlorination of the cooling water is done to control biofouling on cooling system components. However, biofouling is an interfacial problem and bulk dosing of biocide is not only uneconomical but also environmentally unsustainable. What is required is maintenance of a sufficiently large biocide concentration at the water/substratum interface, such that the incoming fouling larvae (less than 1 mm in size) are prevented from settling by repulsion or inactivation. This is difficult to achieve as it requires maintenance of sufficiently high biocide levels near the surface, leaving the rest of the bulk water practically biocide-free. Nevertheless, this can be accomplished if we can modify the surface or pre-load it to release a biocide in a controlled and sustained manner. This would prevent biofouling/biofilm formation at the surface, even if the concentration of the active ingredient in the bulk medium remains low. The same principle can be applied for prevention of biofilm formation on a human body implant. High localized concentration of an antibiotic can prevent/eradicate biofilms on surfaces, there being no necessity to maintain a high body fluid concentration. Following this approach, we have been attempting to develop

polymer based composites and coatings which would prevent microbial attachment without adding undesirable antimicrobial load to the bulk system.

Polymer coating made of enzyme-antibiotic composite

Medical devices coated with antibiotics to control bacterial growth are commercially available. However, they provide only short-term control because of non-uniform antibiotic release profile. Hence they cannot be used for indwelling implants, which require longer implantation. Since they do not ensure sustained release of the antimicrobial, biofilm control becomes difficult. Sporadic release of antibiotic can lead to development of antibiotic resistance among microbes. Antibiotic dosage is usually designed based on killing of planktonic (i.e., free-floating) form of bacteria; the dose is usually inadequate for bacteria in the biofilm mode of life. When the dose is insufficient, the planktonic bacteria may be killed, but those in the biofilm are largely left intact. The polymer system we have developed releases the antibiotic in a sustained manner for a predetermined time period (hours to days). Polycaprolactone (PCL) is an FDA-approved polymer that is biodegradable, bio-absorbable and compatible with many drugs. An antibiotic embedded within PCL will be released based on the degradation rate of the PCL matrix. By controlling the degradation rate, we can also control the drug release rate. To achieve this, we embedded the PCL degrading enzyme lipase in the PCL matrix, which was co-embedded with a model antibiotic, gentamicin. The resulting lipase-gentamicin impregnated in PCL (LGIP) functions in the following manner: lipase uses PCL as its substrate, leading to its degradation, with concomitant release of gentamicin from the polymer matrix. LGIP (in solution form; Fig.1A) could be successfully fabricated in the form of coating on glass surfaces (Fig.1B), as coating on silicone surfaces of Foley urinary catheters[3] (Fig.1 C), as a scaffold (Fig.1D) or as thin sheets[4](Fig.1E). The degradation of PCL proceeds from "inside out" by the formation of pores

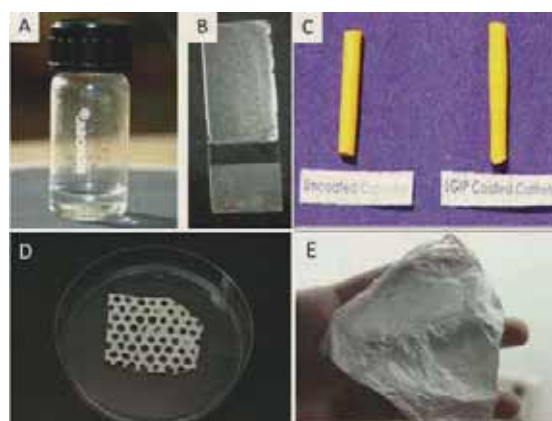Fig. 1: Photographs of lipase-gentamicin impregnated poly-å-caprolactone (LGIP) prepared by various techniques. (A) LGIP in solution ; (B) coating on glass slide by solution casting; (C) dip-coating on Foley urinary catheter; (D) as a scaffold and (E) as thin electrospun sheets.

(Fig. 2B,D) compared to the control polymer (Fig.2A,C), revealing that lipase activity in the polymer matrix remains intact. LGIP showed exceptional antimicrobial efficacy against three test isolates viz., *Staphylococcus aureus*, *Pseudomonas aeruginosa* and *E. coli,* as shown in Fig. 3(A-F). Zones of inhibition observed in culture plates loaded
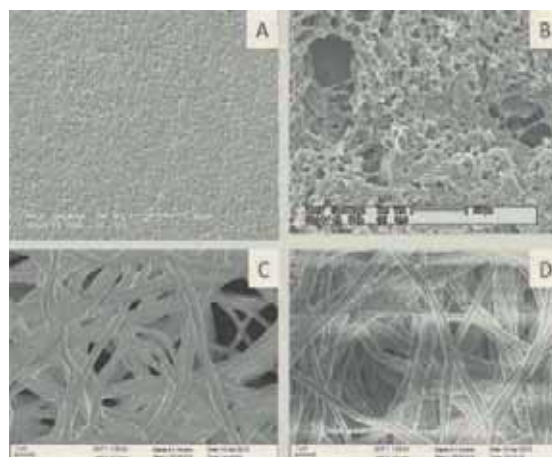

Fig. 2: SEM images of (A) control coating; (B) LGIP coating; (C) Control e-spun sheet; (D) LGIP e-spun sheet undergoing degradation. Images were taken on d 10 of incubation at 37°C in phosphate buffer saline (pH:7.2). Control coating contained only antibiotic and no enzyme. Note the holes in the LGIP film and sheet, formed as a result of enzyme attack from within.
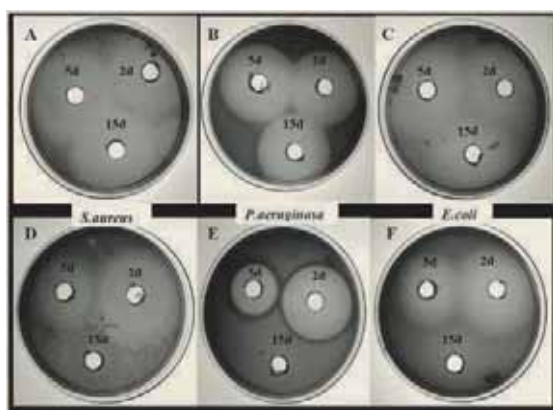
Fig. 3: Antibacterial activity of extracts released from degrading LGIP (A-C), and from control films containing only antibiotic, no lipase (D-F) against three bacterial isolates after 2, 5 and 15 days of incubation. A & D: S. *aureus*, B & E: *P. aeruginosa*, and C& F: *E. coli*
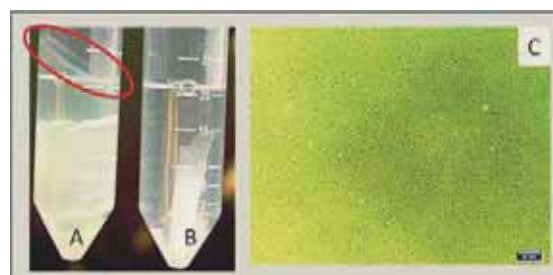

Fig. 4: *E. coli* growth in presence of control film (A) and LGIP film (B) after 10 days of incubation at 37°C (growth medium was replaced every day). Control polymer contained only antibiotic and no enzyme. Red circle in control tube (A) shows the growth of biofilm at the water-air interphase. This is not seen in tube B (containing LGIP). Biocompatibility evaluation of LGIP, showing L929 cell proliferation after 8 h of incubation at 37°C and 5% CO_2 (C).

with LGIP were equal in size (Fig. 3A-C) when compared to those in control plates (Fig. 3D-F), clearly indicating that gentamicin was uniformly being released from LGIP. Throughout the life-time of the coating, gentamicin release remained above the Minimum Inhibitory Concentration (MIC) required to inhibit all the test isolates[3]. *E. coli* showed heavy biofilm growth after 10 days of incubation in presence of control (Fig.4A), while no growth was seen in cells exposed to LGIP (Fig. 4B). Cytotoxicity experiments with LGIP using L929 mouse fibroblasts revealed that the cells were able to attach and adhere to LGIP, pointing to its biocompatibility (Fig.4C).

Our results showed that by manipulating lipase loading, we can control polymer lifetime and gentamicin dosage (Table 1). An initial loading of 9U lipase/g of PCL corresponded to 16 d and a loading of 36 U lipase/g of PCL corresponded to 36 h of PCL life-time. By increasing lipase loading 4-fold (from 9U/g to 36U/g of PCL), a 15 fold increase in GS release was obtained. Moreover, by manipulating the amount of GS in the film (13 and 4 mg of complex/g of polymer), while keeping the lipase loading constant, two different antibiotic release rates could be obtained. Our results suggest that LGIP can be tuned as per clinical requirements and can be used as programmable self-degrading antimicrobial biomaterial for various biomedical applications.

Nitrogen oxides releasing wound dressings for infection control

Apart from implant associated biofilm infections, microbial infection in wounds poses serious health problems, especially in ulcerous non-healing

Table 1: Life-times and antibiotic dose release rates obtained with LGIP coatings.

Enzyme loading, U enzyme complex/g of polymer	Antibiotic loading, mg complex/g of polymer	Dose rate (mg/ml/d)	Life-time (d)
9	13	0.3	16
9	4	0.02	16
36	13	4.5	1.4
36	4	0.04	1.4

wounds. Chronic wounds are generally characterised by the presence of multimicrobial (bacteria, fungi and yeasts) biofilms, necessitating the application of broad spectrum antimicrobials. Moreover, the antimicrobial should be penetrative to kill organisms living deep inside the biofilm. To address these two challenges, we have a developed a nitrogen oxides$_{(g)}$ releasing dressing based on acidified sodium nitrite (ASN)[5]. Acidification of nitrite *in situ* produces nitrous acid, which generates oxides of nitrogen, including NO, N_2O_3 and the nitrosating agent NO^+. Nitrogen oxides (NOs) are effective in killing pathogens, presumably by the generation of nitric oxide and its derivatives collectively known as 'reactive nitrogen species'. Moreover, NO is known to facilitate wound healing. Though simple in its concept, no delivery systems for ASN are commercially available, except for ASN based creams, which have certain limitations[5]. The NOs releasing wound dressing we have developed consists of citric acid linked cotton gauze embedded in a gelatin matrix which is irradiated for cross-linking and sterilization. At the time of application, it is immersed in sodium nitrite solution, leading to release of NOs$_{(g)}$. Laboratory results have shown that the dressing (Fig. 5A) is highly effective against all the tested isolates viz., *E. coli*, *P. aeruginosa*, *Staph. epidermidis*, *Staph. aureus* and the yeast *Candida*

albicans. It is able to bring down the microbial load from 10^6 CFU/ml to nil in 12 h (Fig.5B). The dressing (sterile, lyophilized) can be stored at 37°C and 85% humidity for one year, without any loss of activity. This is significant in the case of poor countries, where transportation and storage facilities are limited. The dressing provides favourable wound healing environment and virtually pain-free wound examination as well as dressing removal.

Chlorine dioxide releasing polymer for biofilm and biofouling control

The above mentioned products have predominant application in the medical field. To address the issue of biofouling control in industrial settings, we are developing a chlorine dioxide releasing polymer system. Chlorine dioxide (ClO_2), an oxidising biocide, is considered to be a better alternative compared to other commonly used oxidising biocides such as chlorine. Its oxidation capacity is high; it reacts with organics only selectively (i.e., low biocide demand) and importantly, does not react with organic matter to form harmful disinfection by-products like the trihalomethanes. ClO_2 kills bacteria faster than chlorine and the dose requirement is smaller. Though very effective for biofouling control, it is not being used widely since it is very unstable and has to be generated on-site. We have designed a ClO_2 based
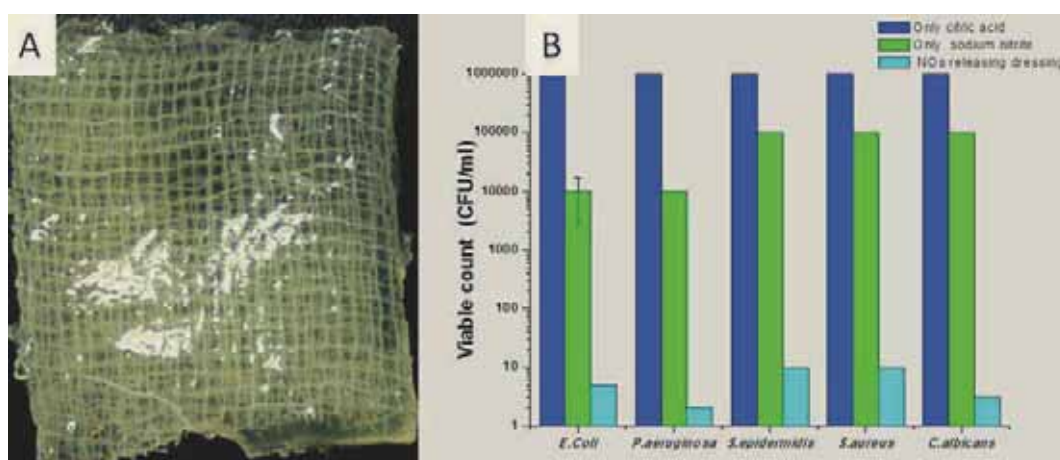

Fig. 5: Photo of nitrogen oxides releasing dressing (A); anti-microbial activity of the dressing tested against five test isolates (B). Bars show killing by citric acid, sodium nitrite and by the dressing.

delivery system, suitable for the control of biofilm and biofouling (Fig.6 A, B). Its antibiofilm activity against *P .aeruginosa* is shown in Fig.6 (C and D). ClO_2 is an EPA-approved biocide for drinking water disinfection and therefore, the product has potential to be employed for domestic drinking water purification. The advantage is that it produces negligible amounts of chlorination by-products (e.g. trihalomethanes), some of which are suspected carcinogens. Therefore, from a health point of view, a chlorine dioxide based disinfection system is a better than a chlorination based system.
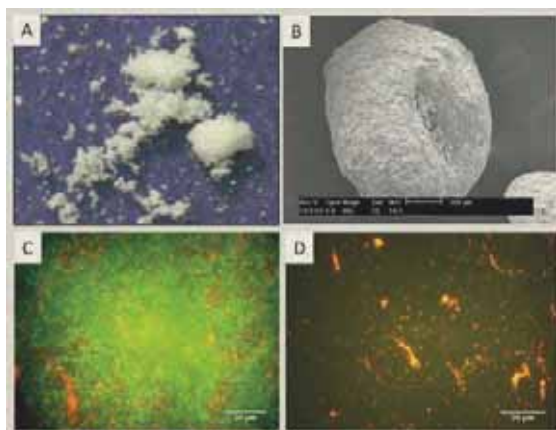

Fig. 6: Photo of ClO_2 releasing polymer (A); SEM image of a single polymer sphere (B); Live-dead imaging of *P. aeruginosa* biofilm after 12 h incubation (C) and after exposing it to ClO_2 releasing polymer (D). Green indicates live and red indicates dead cells. The ClO_2 releasing polymer causes cell killing as well as biofilm removal.

To sum up, microbial biofilms are neither restricted to aquatic environment nor are they important only in cooling water systems of power plants. Biofilm control assumes great importance in the biomedical field as much as in industrial settings. Microbial control strategies outlined here and the products based on such strategies, therefore, have multiple applications. Effective control of microbial biofilms in different environments requires development of innovative solutions, without putting the environment (or the human body) to undue risk.

Acknowledgements

References

1. M. E. Davey, G. A. O'Toole "Microbial Biofilms: from Ecology to Molecular Genetics". *Microbiology and Molecular Biology Reviews*, 64 (2000) 64: 847–867.

2. H.C. Flemming et al. (eds.), "Biofilm Highlights, Springer Series on Biofilms 5", Springer-Verlag, Berlin, 2011.

3. R. Dave, H. Joshi, V.P. Venugopalan. "Novel biocatalytic polymer based antimicrobial coatings as potential ureteral biomaterial: preparation and *in vitro* performance evaluation". *Antimicrobial Agents and Chemotherapy*, 55 (2011): 845-853.

4. R. Dave, P. Jayraj, P. K. Ajikumar, H. Joshi, T. Mathews, V. P. Venugopalan. "Endogenously triggered electrospun fibres for tailored and controlled antibiotic release". *Journal of Biomaterials Science, Polymer Edition.* DOI:10.1080/09205063. 2012.757725 (2013).

5. R. Dave, H. Joshi, V. P. Venugopalan. "Biomedical evaluation of a novel nitrogen oxides releasing wound dressing". *Journal of Materials Science: Materials in Medicine*, 23 (2012): 3097-3106.

Development of Hybrid Micro Circuit Based Multi-Channel Programmable HV Supply for BARC-Pelletron Experimental Facility

A. Manna, S. Thombare, S. Moitra, M. Kuswarkar, M. Punna, P.M. Nair, M.P. Diwakar and C.K. Pithawa

Electronics Division

Abstract

Electronics Division, BARC has developed a Multi channel programmable HV bias supply system for charge particle detector array for use in BARC-TIFR Pelletron-LINAC facility. The HV supplies are compact in size due to use of hybrid micro – circuits developed indigenously and are modular in construction to achieve versatility, scalability and serviceability. All programming operations and monitoring are performed remotely through PC over Ethernet. Each supply has a built-in over voltage, over current and thermal overload protections for safe operation and employs a Zero Voltage Switching (ZVS) technique to reduce thermal stress on the inverter switches. This article describes salient design aspects and performance of the HV supply system.

Introduction

A Multi-channel high voltage system has been developed for biasing Charged Particle Detector Array (CPDA), under commissioning phase in the recently upgraded BARC-TIFR Pelletron-LINAC Facility. This array which consists of 50 detector modules, each comprising of a 400 mm^2, 300 μm thick Si-pad detector and a 10.0 mm thick thallium activated cesium-iodide scintillation detector, will be used for investigations in fusion-fission dynamics, nuclear structure at elevated temperatures, exotic nuclear clusters, and related fields.[1] The HV bias supplies for the CPDA are independently programmable in the range of 0 to 450V with a voltage setting resolution of 1V and 100 μA output current capability. Each supply, called HV channel, has over current, over voltage and thermal overload protection with adjustable ramp rate control facility. As shown in Fig. 1, the supplies, made modular in construction for scalability and maintainability, are accommodated in groups of three 16- channel HV modules in a 4U height, 19" bin, called HV crate. Each HV crate is networked to a host PC using a 10/100Mbps Ethernet for remote control, monitoring and system debugging.

Due to the board complexity of HV modules containing very large number of miniaturized surface mount devices (> 1500 per board); considerable difficulties were faced during the assembly and testing of the first prototypes. To overcome these constraints, a set of Hybrid MicroCircuits (HMCs) have been developed for various functional blocks of the HV supply in collaboration with ECIL, Hyderabad. This has resulted in more than 75% reduction in the number of components onboard along with other benefits such as high reliability, protection from environmental degradation and better high voltage insulation.

Large turn ratio of transformers, normally encountered in HV supplies, exacerbates its parasitic non-idealities. This results in voltage and current spikes in inverter circuit components, worsening switching losses and noise. To improve power efficiency and lower switching noise of the inverter, a ZVS technique has been employed in the design. Control firmware for the crate and HV modules have been developed using a real time operating system (Keil RTX Tiny OS) to meet the requirement of fast

system response. PC based console software has been developed that provides user interface to configure and operate multiple HV crates. The user interface continuously displays the HV readings obtained from 48 channels of a selected crate in a grid.

As many multi detector physics experiments require bias supplies for photomultiplier tubes, a HV system with output voltage capability of up to 2.2KV @ 1 mA has also been developed in the same form factor.

System Description

Each high voltage crate comprises a Low Voltage (LV) dc power module and three 16-channel high voltage modules (Fig. 3). All the dc supplies required for crate powering are generated inside the LV module from 230V ac input. A crate controller with Ethernet interface performs the task of control and data communication with the host PC. Each high voltage module, consisting of 16 HV cards and a controller card, share a local I^2C bus for remote programming and monitoring. The crate controller receives control commands from the host PC via Ethernet and re-addresses it to the respective HV module on the local I^2C bus for execution.

The HV supplies in a module are built on plug-in cards for easy serviceability. An on-board micro-controller (Philips 80C552) with associated control / interface circuitry (Fig.4) executes voltage programming of all the 16 HV channels as per the

external control command. The output voltages and load currents are read back via a set of multiplexers and an ADC. In case of an over-voltage or an overload conditions, independent protection logic shuts down the corresponding HV channel. Over voltage limit is adjustable through hardware and is same for all the supplies on a module. In addition, each 16-channel HV module has a thermal overload protection for safe operation.

The module firmware has provisions to accept control commands through either a RS-232C serial port or the local I^2C bus. The RS-232C port allows isolated testing of the HV module by issuing various system debugging commands from a PC hyper terminal directly. Each module has been provided with 56 hardware monitoring parameters for remote fault diagnosis.

Each HV channel is built using four HMCs; namely, error amplifier, voltage multiplier, voltage / current sense buffer and the inverter driver. These HMCs were developed in Electronics Division to achieve compact, modular hardware with better high voltage insulation. As shown in Fig. 5, the multiplier hybrid contains a two-stage Cockcroft-Walton circuit, an output filter and a surge protection network. The latter network offers protection to the HV load current measuring buffer from induced voltage spikes, due to occurrence of any high voltage transients at the output. The voltage / current sense hybrid comprises of a voltage follower for buffering

Fig. 1: A 48-channel High Voltage crate
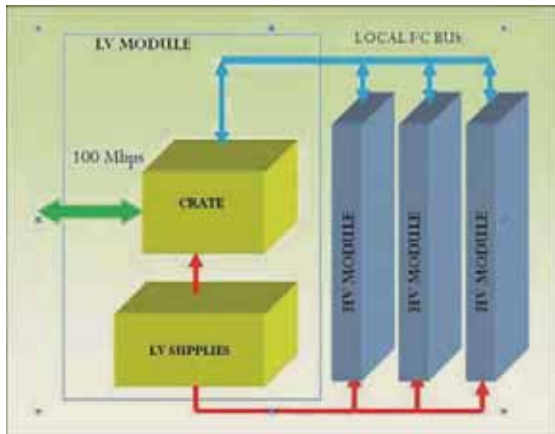

Fig. 2: A 16-channel HV module

Fig. 3: Block Diagram of a 48-Channel High Voltage Module.

Fig. 4: Block Diagram of a 16-Channel High Voltage Crate.

the high impedance HV feedback signal and a current to voltage converter with a polarity changer for measuring the load current flowing out of the supply terminals.

The error amplifier hybrid compares the feedback signal with the HV reference and controls the series pass element (M1) to maintain the HV supply at the desired value. Terminals for external loop compensation and level shifting are provided so as to tailor its use to specific applications. The over-voltage / over-current protection circuitry ensures stress-free operation of the HV supply and also
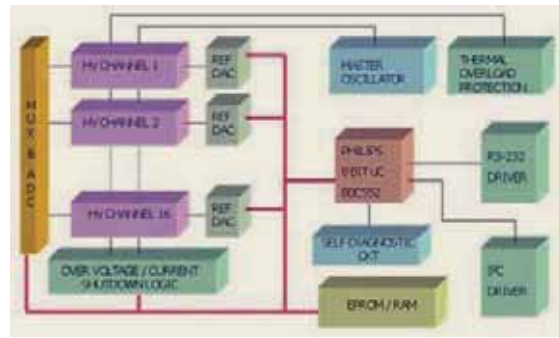
generates a shutdown logic signal under abnormal conditions. The selectable gain inversion block ensures negative feedback signal in the loop for both polarity of HV supply. The inverter driver hybrid contains MOSFET switches for driving push-pull inverter transformer. The turn on / off period of the drivers are slew rate controlled so as to reduce switching noise in the supply.

Salient Design Feature

Voltage and current spikes, generally encountered in switching circuits, worsens power efficiency and noise performance of an inverter. In case of high voltage inverters these problems are further
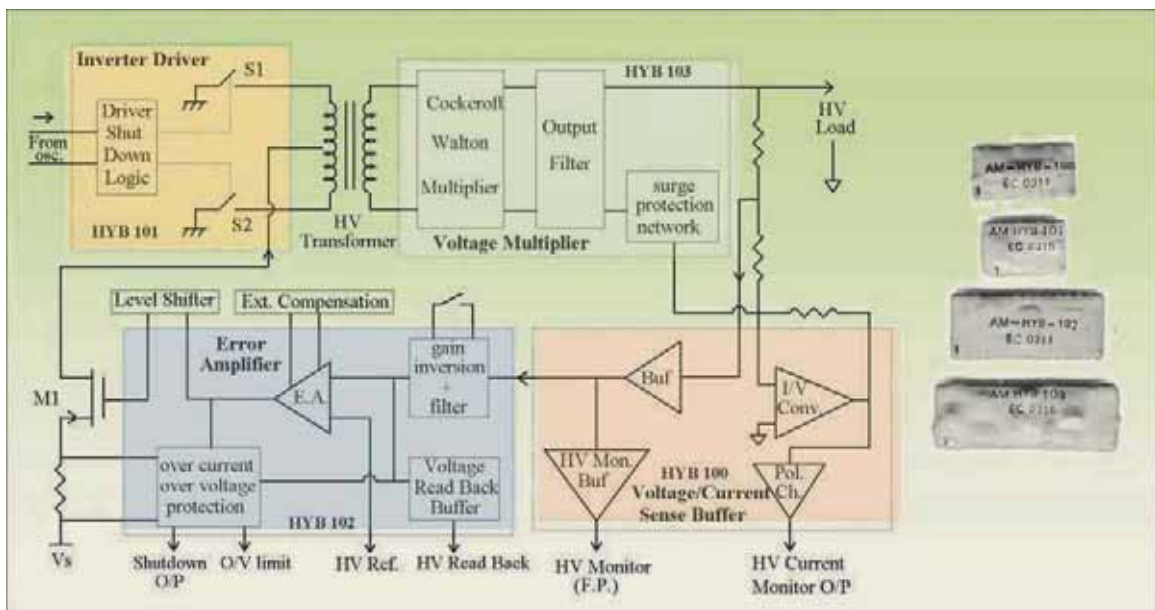

Fig. 5: Block Diagram of a single channel of High Voltage supply with HMCs

aggravated due to the large turn ratio of the transformers. A ZVS technique that has been used in the HV supplies to mitigate these problems is described below.

Zero Voltage Switching (ZVS) inverter: The high voltage transformers in general have significant parasitic capacitance that should be charged resonantly so as to reduce thermal stress on the switches. For a transformer made with ferrite pot core, the lumped secondary parasitic capacitance can be approximated as,

$$C_s = \frac{4}{3N} \frac{\varepsilon \cdot L \cdot \pi}{\cosh^{-1}\left[\dfrac{h+2r}{2r}\right]} \qquad (1)$$

Where N is the number of layers in the secondary winding; ε, h are permittivity and thickness of the interlayer insulation, L is mean length of one layer of conductor and r is the conductor radius. As shown in Fig. 6, the magnetizing inductance and the parasitic capacitance of the transformer form a resonant network. The switches, S_1 or S_2 are turned on when the voltage across them is zero. For a constant frequency fixed duty cycle operation with on time 't_0', the rise time t_r of the voltage waveform (Fig. 6) across each switch is given by,

$$t_r = \frac{2}{\omega_r} \cdot \tan^{-1}\left[\frac{2}{\omega_r \cdot t_0}\right] \qquad (2)$$

Where $\omega_r = 1/(L_s C_s)^{1/2}$ is the resonant frequency of the transformer, L_s being the magnetizing inductance, reflected to secondary side. As t_r is independent of E, the input voltage of the inverter, the resonant operation is maintained throughout the operating range of the supply by selecting an appropriate fixed duty cycle. The C_s and L_s are controlled by adopting uniform winding procedure and air-gapped ferrite core respectively for the transformer.

Performance / Discussion

Based on this design, 240 HV supplies were constructed using the hybrid microcircuits. Some of the observed performances of the HV supply are:
• Ripple voltage at full load $<$ 100 mV (p-p).
• Load regulation better than 0.01% of F.S. HV
• Long term drift: less than 0.02 % in 24 hrs.
The step response (5 mV step at the HV ref input) of the supply was measured to have a rise time of about 340 μs with a peak overshoot of 35%.

Each hybrid microcircuit was constructed with two ceramic substrates, sandwiched with components mounted on both the sides, so as to reduce their overall sizes. Existence of significant parasitic coupling was noticed between the ac capacitors and the output filter section of HV multiplier hybrid, worsening the output ripple. The problem was addressed by careful layout of the components on the hybrid with the help of electrostatic simulations and providing a ground plane between these two
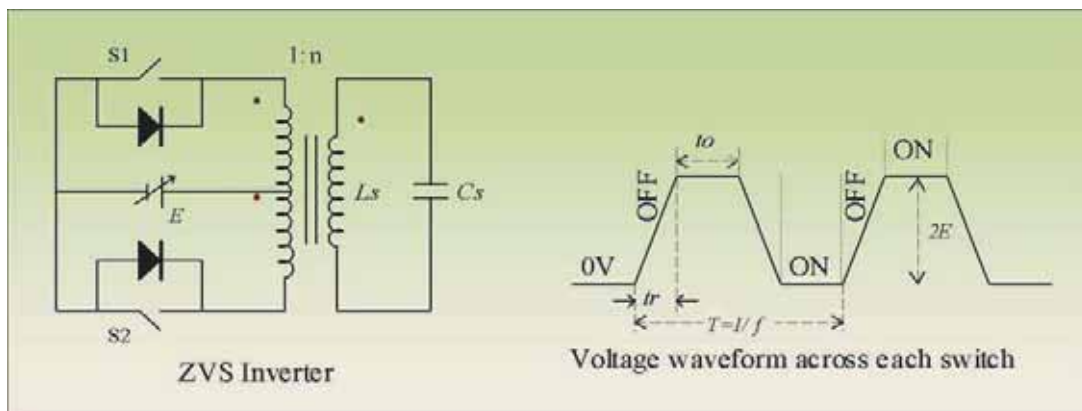

Fig. 6: The ZVS inverter with voltage waveforms across each switch

sections of the multiplier circuit. All the sensitive tracks on the hybrids were guarded so as to reduce errors due to leakage currents.

Conclusions

A zero voltage switching technique, insensitive of load and operating voltages, has been used in the HV inverter to resonantly charge the transformer parasitic capacitance at frequencies in excess of 60 kHz. This has resulted in reduction of switching losses and low noise in the supply.

In order to achieve very compact size for the multi channel high voltage modules with easier assembly, testability and high reliability, it was found advantageous to build hybrid microcircuit based HV supplies. Reduction in component count thus achieved has significantly reduced board complexity with added benefits such as protection from environmental degradation, better high voltage insulation due to epoxy coating and improved thermal management. These HMC's can be used as building blocks to generate both polarity HV outputs covering various detector biasing applications.

Acknowledgement

References

Bency John et. al, "Charged particle identification by pulse shape discrimination with single-sided segmented silicon-pad detectors", *Nuclear Instruments and Methods in Physics Research* A 609 (2009) 24–31.

12ᵗʰ ISMAS-TRICON-2013 : a Report

The Indian Society for Mass Spectrometry (ISMAS), with its office at Fuel Chemistry Division, BARC, organized the 12ᵗʰ ISMAS Triennial International Conference on Mass Spectrometry (12ᵗʰ ISMAS-TRICON-2013) at Cidade-de-Goa, Dona Paula, Goa during March 3 - 8, 2013.

Prof. S. Shetye, Vice-Chancellor, Goa University delivered the inaugural address. Prof. S.K. Aggarwal, President ISMAS and Chairman, Organizing Committee of 12ᵗʰ ISMAS-TRICON-2013, delivered the welcome address. Sh. P.G. Jaison, Treasurer, ISMAS and Convener, Organizing Committee, highlighted the scope of the Conference. Sh. Vijay M. Telmore, Secretary, Organizing Committee, proposed a vote of thanks. Prof. J.N. Goswami, Director, Physical Research Laboratory, Ahmedabad, delivered a key-note Address on "*The first ten million years of the Solar System*".

Dr. S. Prabhakar, Indian Institute of Chemical Technology, Hyderabad, Prof. T. Pradeep, Indian Institute of Technology Madras, Chennai and Prof. A.K. Tyagi from Indira Gandhi Centre for Atomic Research, Kalpakkam. were honoured with "EMINENT MASS SPECTROSCOPIST" awards.

Dr. Jobin Cyriac, Indian Institute of Space Science and Technology, Thiruvananthapuram, Dr. V. Sabareesh, Vellore Institute of Technology University, Vellore and Dr. Wahajuddin, Central Drug Research Institute, Lucknow. were honoured with "YOUNG MASS SPECTROSCOPIST" awards.

32 contributed papers were presented as posters in two different sessions and were classified into different areas like (i) Atomic and Molecular Physics-AMP, (ii) Biological and Environmental Sciences- BES, (iii) Earth and Planetary Sciences – EPS, (iv) Isotopic Composition and Concentration Measurements – ICC, (v) Instrumentation – INS, (vi) Nuclear Technology (NT) and (vii) Organic Chemistry – OC. In addition, there were oral presentations by Instrument manufacturers to highlight the latest advances in MS instrumentation for various applications in different areas of science and technology. The Conference also provided a forum for young researchers to make oral presentations.

On the dais from left to right: Mr. P.G. Jaison, Treasurer, ISMAS and Convener, Organizing Committee, Prof. J.N. Goswami, Director, Physical Research Laboratory, Prof. S.K. Aggarwal, President, ISMAS and Chairman of the Organizing Committee, Prof. S. Shetye, Vice-Chancellor, Goa University and Mr. Vijay M. Telmore, Secretary, Organizing Committee

IPA – BARC Theme Meeting on Synergy in Physics and Industry: a Report

The Government of India has proposed a new Science, Technology and Innovation Policy as a part of decade of Innovation announced earlier. Synergy between Physics and Industry is crucial for the success of this endeavor. With this in focus, the Indian Physics Association and Bhabha Atomic Research Centre jointly organized a theme meeting entitled "Synergy in Physics and Industry" during January 21-23, 2013 at BARC. The purpose of the meeting was to suggest ways to enhance the cooperation between the academic institutes and the industry and highlight the role of national labs in bringing the synergy amongst the three. With this motivation three plenary talks (representing National Laboratory, Industry and Academic institutes) were organized. Dr. A. Kakodkar (national lab-DAE) spoke on Translation of research in deployable applications. He pointed out that there is lack on confidence in industry towards academic institutes and vice versa. A possible way to improve this confidence is to encourage movement of personnel between industry and research institutes and to enable dual affiliation. Shri K. R. S. Jamwal (industry- Tata Industries) gave a talk on Industry academia relationship- bridging the gap. He stressed that Indian industry has limited manufacturing based on latest scientific developments and technologies. Industry often depends on proven and usually obsolete foreign technology. Innovative research inputs to industry are necessary to change this situation. Dr. R. Banerjee (academic institute – IIT(B)) spoke on Synergizing Industry – Academia Linkages: An academic perspective. He compared data for different countries and showed that in India research is predominantly funded by Government with very little contribution from Industry. He pointed out that

India's rank is 50th for academia-industry collaboration and 59th (per million population) towards generation of useful patents. He suggested that these need to change in order to improve quality of research and its utilization in Industry. The meeting further focused on the following topics: Energy; Automobiles; Medical diagnostics and devices; plasma and micro-fabrication technology. Several invited talks related to the above theme areas, from the experts belonging to National labs, industry and academic institutes were organized. The highlight of the meeting was a panel discussion on Synergy in Physics and Industry chaired by Dr. R. Chidambaram with panelists from all the three organizations. In his remarks to initiate panel discussion, Dr. R. Chidambaram mentioned that an important area where capabilities of Indian industry need to be built up is precision engineering and instrumentation for mega science projects as accelerators and research reactors. Such collaboration will also enhance industry-academia interaction for taking up additional challenges. He mentioned that in advanced countries an equilibrium exists in knowledge being developed in academic institutes and that transferred to industry. Enhancement in academia-industry interaction is necessary to establish similar developments and smooth transfer of technology to industry in India. Similar views were expressed by other invited speakers and panel members.

The participants were unanimous in appreciating the timeliness of this theme meeting and in fact suggested that this kind of meeting should be repeated in other parts of the country and also covering other themes.

2nd International Symposium on Neutron Scattering (ISNS 2013): a Report

The 2nd International Symposium on Neutron Scattering (ISNS 2013) was held at the Training School Complex, Anushaktinagar, Mumbai, during January 14-17, 2013. It was sponsored by the Board of Research in Nuclear Sciences, The symposium was organized by BARC in association with the Neutron Scattering Society of India. The symposium was inaugurated by Shri Sekhar Basu, Director, BARC. Dr. S. Kailas, Director Physics Group, BARC presided over the inaugural function. The first ISNS was held at Mumbai in January 2008.

The symposium covered all aspects of neutron scattering including neutron scattering facilities, instruments, science and applications. A particular emphasis was given on the application of neutrons in studies of energy storage, batteries, functional materials, and soft matter, besides simulation of experiments, and detectors.

There were more than 200 participants including several world leaders from laboratories in various countries. There were 50 invited talks, 18 oral presentations and 87 poster presentations. Within the category of the invited talks, there were 13 presentations on neutron scattering facilities which covered almost all present day mega-facilities like, ILL (France), ISIS (UK), J-PARC (Japan), and ORNL (USA). Besides others important facilities, namely, FRM II (Germany), PSI (Switzerland), LLB (France), JINR (Russia), ANSTO (Australia), JCNS (Germany), KAERI (Korea) and BARC (India) were also covered. The details of the upcoming facility of European Spallation Neutron Source (Sweden) were also presented. The remaining 37 talks were presented in parallel sessions, which covered a wide range of science that is being pursued all over the world.

Researchers from various universities and other academic institutions utilize the National Facility for Neutron Beam Research at BARC regularly. This international symposium enabled very useful scientific discussions among the national and international neutron scattering researchers.

The XV School on "Neutrons as Probes of Condensed Matter" was also organized prior to the ISNS jointly by BARC and UGC-DAE-CSR during January 8-12, 2013.

Shri Sekhar Basu, Director, BARC releases the brochure on the National Facility for Neutron Beam Research during the inaugural function of the ISNS 2013. (From left) Dr. S.M. Yusuf (Local Convener, ISNS 2013), Dr. S. Kailas (Director, Physics Group), Shri Sekhar Basu (Director, BARC), and Dr. S.L. Chaplot (Head, SSPD, and Chairman Organizing Committee, ISNS 2013).

Eighteenth National Symposium on Environment (NSE-18): a Report

The Eighteenth National Symposium on Environment (NSE-18), was organized at JNTUA, Anantapur, AP during March 11-13, 2013, jointly by the Health Safety & Environment Group, BARC and JNTUA. This was sponsored by BRNS, DAE. The focal theme was "Current Perspectives on Environmental Protection". In all 125 contributed papers were presented during the symposium. These included papers from various universities and institutions and by scientists from various DAE units involved in the field of environmental studies. The topics broadly covered Environmental Radioactivity and Protection, Environmental Modelling, Environmental Monitoring and Assessment, Radioecology, Mitigation of Environmental Pollutants, Advanced Instrumentation for Environmental Monitoring, Hydro-geochemistry and Speciation Studies, Flora and Fauna, Demographic Studies among others.

The idea behind holding this symposium at Anantapur was its proximity to the uranium mining and processing project of UCIL, DAE at Tumalapalle. The symposium was inaugurated by Shri. D. Acharya, CMD, UCIL, as Chief Guest. Shri Acharya appraised the delegates about the various aspects of uranium mining and nuclear power generation. He assured the participants that enough experience exists in the country on these activities and the operation of uranium mining and processing at Tumalapalle is absolutely safe for occupational workers as well as for the population residing in nearby areas.

A one day workshop along with symposium was also held, especially for the benefit of students and faculty of various universities. The workshop covered many relevant topics of monitoring and modeling of various environmental matrices, including radioactivity, trace elements, organic chemicals etc. A session on career prospects and research collaboration in DAE was also dedicated for the benefit of the students and other participants. The response to the program was overwhelming and the students and faculty participated in the discussions very actively.
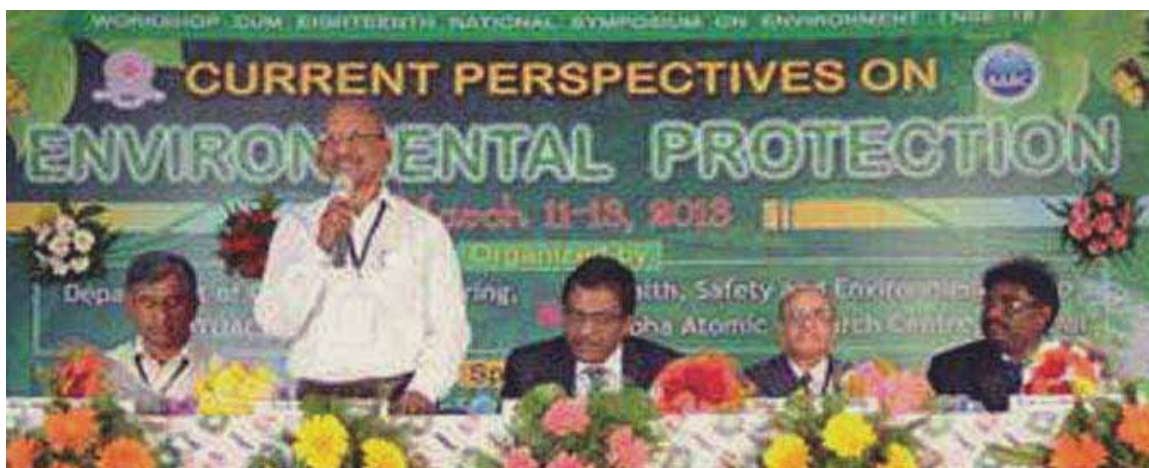
From Left to Right: Shri. V.D. Puranik (Head, EAD, BARC – Co-Chairman of organizing committee); Prof. D. Subba Rao, Vice-Principal, JNTUACE; Shri. D. Acharya, C&MD, UCIL, Jaduguda (Chief Guest); Prof. K. Lal Kishore , Vice Chancellor, JNTUA (Guest of Honour), Prof. S.V. Satyanarayana (Principal, JNTUACE, Pulivendula- Chairman of organizing committee)

Twenty First National Laser Symposium (NLS-21): a Report

The twenty first edition of National Laser Symposium (NLS-21) was organized by the Laser & Plasma Technology Division of Bhabha Atomic Research Centre during February 6 - 9, 2013 at NPCIL, Mumbai. The symposium was inaugurated on February 6, 2013, by Shri Sekhar Basu, Director, BARC. In his inaugural speech, Shri Basu highlighted the applications of lasers in various programmes of DAE in general and in the nuclear programme in particular. The symposium keynote address was delivered by Dr. Ajoy Ghatak, formerly professor of physics at IIT Delhi, an eminent laser physicist and author of many books that have become popular among the student and research community alike. In his address, Dr Ghatak gave a glimpse of the historical evolution of fibre laser.

The symposium, which was attended by over 500 delegates, was quite inter-disciplinary with topics ranging from 'physics and technology of lasers to 'lasers in nuclear technology, defense, space, medicine, industry, and environment'. There was an enthusiastic response from contributors, invited speakers and industry. Financial support was provided to many deserving research students to facilitate their participation at the symposium. The symposium included 10 regular scientific sessions comprising of 7 plenary and 17 invited talks by a talented blend of senior and young researchers from India and abroad. There were 3 poster sessions consisting of a total of 277 contributory papers selected from over 350 submissions, highest to date for any NLS, 2 doctoral presentation sessions that included 7 oral presentations of recent PhD theses on related topics. The poster sessions were very inspiring with active participation from both young and senior researchers. The Indian Laser Association (ILA), like every year, had organized industrial exhibition of lasers and laser related products during the symposium that was also inaugurated by Director, BARC.

ILA, co-sponsor of the symposium, organised three short tutorial courses viz., (a) Advances in Tunable Lasers, (b) Fast and Ultrafast Laser Spectroscopy, and Molecular Dynamics, and (c) Photonics on Feb 4 and 5, 2013, immediately preceding the symposium. While the first two courses were conducted in the Training school complex, Anushaktinagar, the third course was held in TIFR, Colaba. These courses were attended by more than 100 young researchers from all over the country.

Dr. S. G. Markandeya, Controller, BARC, presided over the concluding session on February 9 and gave away the best thesis and poster awards.

Director, BARC, delivering the inaugural address of NLS-21

National Workshop on "Non Destructive Evaluation on Structures (NDES-2013): a Report

A Two-day National Workshop on "Non Destructive Evaluation on Structures (NDES-2013)" was jointly organized by the Association of STructural Rehabilitation (ASTR) and the Indian Society for Non Destructive Testing (Mumbai chapter) under the aegis of Bhabha Atomic Research Centre & Homi Bhabha National Institute during March 8-9, 2013 at Multi Purpose Hall, BARC Training School Hostel, Anushaktinagar, Mumbai.

ASTR and Indian Society for Non Destructive Testing are professional bodies involved in the propagation of structural and NDT related knowledge amongst Engineers, Scientists, Technicians working in various industries and academic institutions.

This seminar was aimed to assess the health of concrete and steel structures by using non destructive evaluation methods such as Rebound Hammer, Ultrasonic Pulse Velocity, Thermography, Low Amplitude Vibration Signals, Corrosion Potentials, Ground Penetration Radar Signal, Radiography etc.

This assessment will help the utility for repairing, retrofitting in case of increased load demand due to

earthquake, fire etc. on the structure. This eventually will help for life extension of the structures.

Approximately 155 delegates participated in the workshop from BARC, NPCIL, BRIT, Heavy Water Board, Universities & Engineering Colleges and Private organizations.

This workshop included invited talks on various subjects and product exhibitions from various firms.

Eminent speakers from BARC, IGCAR, IIT Mumbai, KCCPL, IITGN, L&T, ISNT, ASTR delivered invited talk on more than ten topics related to NDE of structures.

The Workshop was inaugurated by Shri S.S. Bajaj, Chairman, Atomic Energy Regulatory Board. Shri Manjit Singh, Director, DM&A Group, BARC inaugurated the exhibition and the Proceedings were released by Shri K.K. Vaze, Director, RD&D Group, BARC. All delegates were given participation certificates during Valedictory Function organized at the end of the workshop on 9th March, 2013.

Release of proceedings during inaugural function of NDES 2013.
(From L to R: Dr. G.R.Reddy, Dr. B. K.Dutta, Shri K.K.Vaze, Shri S.S.Bajaj, Shri Manjit Singh, Shri S.P. Srivastava

DAE-BRNS theme meeting on the Physics Aspects of Accelerator Radiation Protection (PAARP)

The Health, Safety and Environment Group organized the PAARP meeting which was held at the BARC Training school hostel, from 20-22 February, 2013. The technical sessions covered the recent developments in the fields of nuclear reaction, Monte Carlo radiation transport, FLUKA Monte Carlo code, dosimetry and shielding benchmark studies, micro dosimetric methods and techniques, safety aspects of radioactive ion beams, ADS and medical accelerators.

The theme meeting was attended by about 75 persons from India. Eminent scientists, 9 from abroad and 14 from India were invited to deliver lectures. Dr V. Vlachoudis (CERN, Swtizerland) and Dr M. Santana (SLAC, USA) held a tutorial on the recent advances and developments in the FLUKA Monte Carlo code. Dr R. Capote (IAEA, Austria) held a tutorial session on the EMPIRE nuclear reaction code.

Inaugural address by Dr. L.M. Gantayet,
Director, BTDG, BARC

Delegates at the PAARP meeting

Director-General, IAEA, Visits BARC

His Excellency Mr. Yukiya Amano, Director-General, International Atomic Energy Agency (IAEA), Vienna visited BARC, Mumbai on March 11, 2013. He inaugurated BARC's Digital Radiotherapy Simulator installed at the Tata Memorial Centre (TMC) at Parel, Mumbai through video-conferencing from the Central Complex (CC), BARC.

A poster exhibition on the theme *Atoms in the Service of the Nation* held at CC auditorium, BARC, was also inaugurated by H.E. Amano during his visit. Young scientists presented R&D work on Societal Applications of Nuclear Energy in the areas of health, environment, food, water, industry and agriculture through posters. During the interactions he appreciated the excellent work done by BARC scientists and engineers in the area of Agriculture and Food and stressed the need to enhance this cooperation in the field of peaceful nuclear technologies. Later the Director General released a brochure "Atoms in the Service of the Nation".

H.E Amano also visited the Tarapur Waste Management Plant (TWMP). A brief presentation was made about the activities at TWMP. He was taken through the Advanced Vitrification System and the Solid Storage and Surveillance Facility and Mr. Amano evinced keen interest in all the activities.

On the occasion of the Silver Jubilee function of the Indian Nuclear Society (INS), H.E. Amano gave a talk on "IAEA Perspectives on the Future of Nuclear Energy" at the Nabhikiya Urja Bhavan, Mumbai. During this presentation, Amano stressed the need to utilize nuclear power for improving energy security, reducing the impact of volatile fossil-fuel prices and thereby mitigating the effects of climate change. He also appreciated the generous Indian support to the Program of Action for Cancer and made a special mention about the donation of Bhahbhatron II radiotherapy machines to Vietnam and Sri Lanka.

Inauguration of BARC's Digital Radiotherapy Simulator by H.E. Yukiya Amano, Director General, IAEA

BARC Scientist explaining the poster to H.E. Yukiya Amano

H.E. Yukiya Amano releasing the brochure "Atoms in the Service of the Nation"

H.E. Yukiya Amano visiting the Tarapur Facilities

Workshop on
Very High Energy Gamma-Ray Astronomy :
a Report

A Workshop on Very High Energy Gamma-Ray Astronomy was organized by the Astrophysical Sciences Division at the Gamma-Ray Observatory, Mt. Abu during 28 Jan.-2 Feb., 2013. 16 participants, who were selected out of 40 applicants on the basis of their aptitude and research experience, participated in the 6 day workshop. The participants included 10 doctoral students and 6 M.Sc. final year students from 8 universities and 5 research centres of the country. Lectures, simulation and data analysis sessions were conducted from morning till late afternoon and the experiment sessions were organized during the evenings at the Observatory. The faculty was drawn from ApSD, BARC and TIFR. The workshop was fully funded by the Board of Research in Nuclear Sciences.

Participants and faculty of the Gamma Ray Astronomy workshop held at Mt.Abu

BARC Scientist Honoured

Dr. S.P. Kale, Head, Technology Transfer and Collaboration Division has been honoured with the Padma Shri Award by the Government of India on January 26, 2013 in the Discipline of Science and Engineering. Dr. Kale has developed the NISARGRUNA biogas technology for solid biodegradable waste resource management. This is a combination of aerobic and anaerobic processes for faster and better degradation of biodegradable waste resulting in methane enriched biogas and organic manure generation. He has been propagating the NISARGRUNA biogas concept for solid biodegradable waste resource management at various levels in the country. So far 160 Nisargruna projects have been installed all over the country. These plants are based on kitchen, market, poultry, dairy and abattoir biodegradable waste resources. There are some plants which are working on biological sludge generated in effluent treatment plants of textile industry.

His fields of interest include: Marine pollution, Agriculture Biotechnology, Computer applications, Bioenergy, production of metallic nanoparticles through biological route and creating Public awareness regarding sustainable environment.

BARC Scientists Honoured

Name of the Scientist :	:	**Dr. S. Kailas**
Affiliation	:	Director, Physics Group
Award	:	Elected as Fellow of the Indian National Science Academy
Conferred by	:	Indian National Science Academy

Name of the Scientist :		**Dr. S. P. Chaplot**
Affiliation	:	Head, Solid State Physics Division
Name of the Award	:	Elected as Fellow of the Indian National Science Academy
Conferred by	:	Indian National Science Academy

Name of the Scientist :		**Dr. S. K. Gupta**
Affiliation	:	Head, Technical Physics Division
Name of the Award	:	MRSI Medal for contributions to Material Science & Engineering
Conferred by	:	Materials Research Society of India

Beautiful Yellow Flower Tree in Anushaktinagar
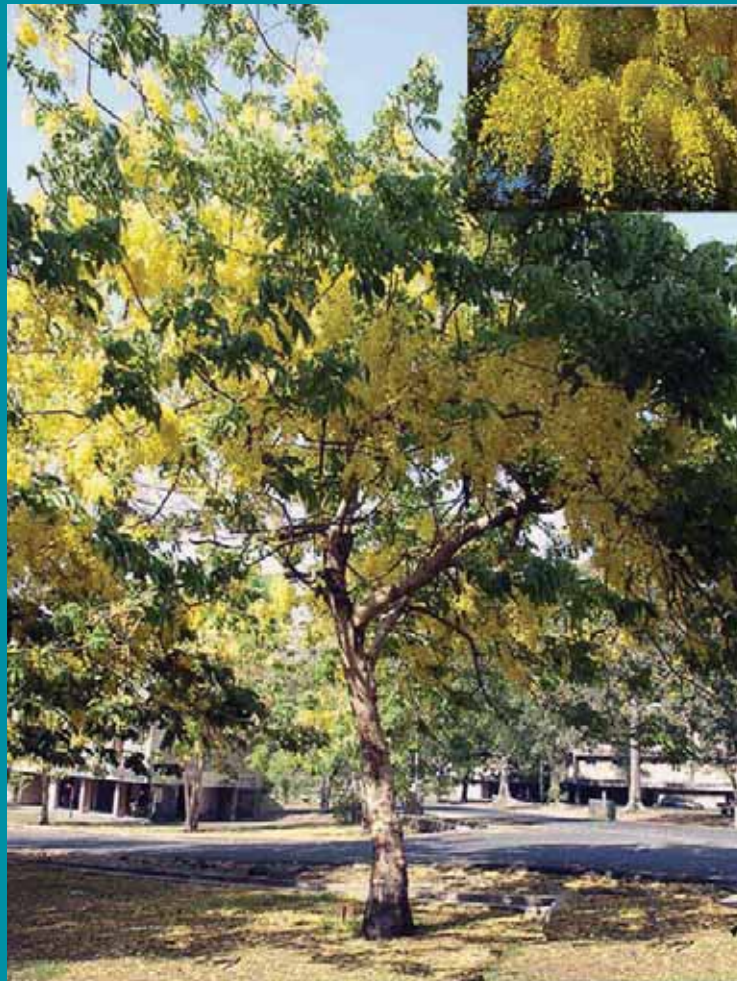
Cassia fistula (Golden shower)

Cassia fistula is a beautiful tropical tree with yellow flowers. It belongs to Family Fabaceae and is known by several names such as, Golden shower, Indian Laburnum, Amaltas and Pudding Pipe Tree. Cassia fistula is native to Indian Subcontinent and other regions of South East Asia. It is an important ornamental plant with medicinal properties and also has cultural significance in South India.

More information can be found at website of
National Tropical Botanical Garden
(http://www.ntbg.org/plants/plant_details.php?plantid=2430)